COUPLING BETWEEN THE PROPERTIES OF SMART MATERIALS AND LIGHT EMISSION

CHEN LI

Ph. D

The Hong Kong Polytechnic University

2017

The Hong Kong Polytechnic University

Department of Applied Physics

Coupling between the Properties of Smart Materials and Light Emission

CHEN Li

A thesis submitted in partial fulfillment of the requirements

for the degree of Doctor of Philosophy

March 2017

CERTIFICATE OF ORIGINALITY

I hereby declare that this thesis is my own work and that, to the best of my knowledge and belief, it reproduces no material previously published or written, nor material that has been accepted for the award of any other degree or diploma, except where due acknowledgement has been made in the text.

_____ (Signed)

CHEN Li (Name of student)

Abstract

Luminescent materials and devices have drawn much attention due to their widely applications in solid-state lighting, light-emitting diodes (LEDs), architectural decoration, digital displays, bio-imagines, optical sensors and lasers. On the other side, smart materials are designed materials which are capable of responding to external stimuli, such as stress, electric or magnetic field, and so on. Herein, the coupling of smart materials and luminescence phenomenon has opened a new path to study luminescence emission and manipulate the spectral properties, and their potential has been developed from basic electronics and optoelectronics to a wide range of applications.

In this thesis, firstly, a type of flexible phosphor composite has been fabricated by mixing metal ion-doped ZnS into Poly(dimethylsiloxane) (PDMS) matrix. By stimulating with a uniaxial strain of stretch and release, white and green light emission can be observed from the flexible phosphor composite. In addition, a kind of piezo-photonic luminescent device has also been fabricated via integrating the

polymer phosphor layer on the top of piezoelectric actuator of $Pb(Mg_{1/3}Nb_{2/3})O_{3-x}PbTiO_3$ (PMN-PT). Light emission from this hybrid device is ascribed to the non-central symmetric crystal structure of wurtzite-type ZnS material, which inherently produces piezoelectric effect under strain. Energy transitions of the observed white light emissions from the phosphor composites and device may originate from the donor acceptor pairs recombination between Al_{Zn}-Cu_{Zn}, as well as the radiation transition between $^4T_1$ and $^6A_1$ of Mn^{2+} ion.

On the other hand, significant tuning photoluminescence (PL) of smart phosphor materials has attracted widespread interest in various research fields, such as optical sensing and information storage. In contrast to traditional chemical approach, we present in-situ and real-time modulation of two kinds of smart phosphor materials in the form of piezoelectric strain and magnetostrictive stress, respectively. By integrating N,N-diphenyl-4-(1,2,2-triphenylvinyl)aniline (DPA-TPE) thin film with PMN-PT substrate or Fe-Co-Ni magnetostrictive composite respectively, the PL intensity of DPA-TPE thin film decreased linearly with the external applied electric or magnetic field. On the contrary, the new emerging

organic-inorganic halide perovskite ($CH_3NH_3PbI_3$) shows a PL intensity enhancement during the application of biaxial piezoelectric strain provided by PMN-PT substrate. The reason may be that the biaxial strain has reduced the surface defects of the perovskite thin film.

In conclusion, we have investigated different mechanical stresses to stimuli light emission from flexible phosphors composite and modulate the PL emission intensity from two types of smart phosphor materials. These findings will aid further research of luminescent materials and show promising application in optoelectronic devices and energy harvesting with various type of mechanical stresses.

List of Publications

1. **L. Chen**, M.-C. Wong, G.X. Bai, W.J. Jie, and J.H. Hao, White and green light emissions of flexible polymer composites under electric field and multiple strains. *Nano Energy*, 14 (2014) 372.
2. M.-C. Wong, **L. Chen**, M.-K. Tsang, Y. Zhang, and J.H. Hao, Magnetic-induced luminescence from flexible composite laminates by coupling magnetic field to piezophotonic effect. *Advanced materials*, 2015, 27, 4488-4495.
3. M.-C. Wong, **L. Chen**, G.X. Bai, L.B. Huang, J.H. Hao, Temporal and remote tuning of piezophotonic effect-induced luminescence and color gamut via modulating magnetic field. *Advanced Materials*, DOI: 10.1002/adma.201701945 (2017).
4. W. Xu, L.B. Huang, M.-C. Wong, **L. Chen**, and J.H. Hao, Environmentally friendly hydrogel-based triboelectric nanogenerators for versatile energy harvesting and self-powered sensors. *Advanced Energy materials*, 2017, 7, 1601529.

5. Y. Chen, Y. Zhang, D. Karnaushenko, **L. Chen**, J.H. Hao, F. Ding, O.G. Schmidt, Addressable and color-tunable piezophotonic light-emitting stripes. *Advanced materials*, 2017, 29, 1605165.

Acknowledgments

I would like to sincerely thank my supervisor, **Prof. Jianhua Hao**, for offering me the opportunity to pursue the Ph. D. degree in Hong Kong, which may have a deep influence in my whole life. During the three and a half years of my study in Hong Kong, he guides me in doing research program, analysing and solving experiment problems with his profound knowledge and patience. He always gives me the most tolerance and optimism with my experiment and study, like a father with deep concern. Besides, his enthusiasm and diligence with his work inspire me to do better in my work. I am grateful for his guidance and supports for me to achieve my doctorial study and make this thesis a reality.

I would like to acknowledge the academic members in our department: Prof. Shu Ping Lau, Prof. Siu Fung Yu, Prof. Jiyan Dai, Prof. Feng Yan, and Dr. Xuming Zhang for their insightful suggestions and supports during my research. Also, I am grateful to Prof. Benzhong Tang from HKUST for his generous assistance in my research work. I want to thank Dr. Hardy Lui, Dr. Wei Lu, Dr. Terence Wong, Dr.

Albert Choy and Dr. Vincent Chan for their help in facility utilization in our department.

I am grateful to Mr. Man-Chung Wong for his assistance in experiment measurements. Without his help, I can't smoothly finish my research. Also, I would like to thank Dr. Gongxun Bai for his guidance on the luminescence spectrum measurement and many suggestions in my study. I am also grateful to Dr. Wenjing Jie and Dr. Huihong Lin for their suggestions in my study and company in the last three years. I am grateful to Mr. Peng You for his great help in fabrication perovskite thin film and devices which benefits me a lot in my experiment. I would like to give my thanks to Mr. Weijun Zhao from HKUST for his help in offering the AIE sample used in my research work. I would also like to thank Mr. Zhibin Yang for his help in sputtering electrodes and electrical measurement. I am grateful to my other group members Dr. Longbiao Huang, Mr. Wei Xu, Mr. Ming-Kiu Tsang, Mr. Shuoguo Yuan, Dr. Yang Zhang and Dr. Wen Huang for their help and suggestions in my experiment and study.

I am so honored to get so much help and assistance from Dr. Zhike Liu, Dr. Chao Xie, Mr. Guanqi Tang, Mr. Naixiang Wang, Dr. Meng Zhang, Dr. Ning Wang, and Mr. Qingming Chen.

Besides, I want to give my sincere thanks to Ms. Xuting Sun, Dr. Shan Guo, Dr. Xiaowen Huang, Ms. Yujiao Zhu and Mr. Zhiyong Wang for their friendships, company and encouragement in my study and life in the last four years in Hong Kong.

Finally, I would like to express my appreciation and love to my parents and my elder sister for their unwavering and unconditional love throughout my life.

Table of Contents

List of Figures

List of Tables

List of Acronyms

Acronyms	Description
PL	Photoluminescence
EL	Electroluminescence
ML	Mechanoluminescence
EML	Elastico-mechanoluminescence
TFEL	Thin film electroluminescence
CB	Conduction band
VB	Valance band
PMN-PT	$Pb(Mg_{1/3}Nb_{2/3})O_{3-x}PbTiO_3$
PVDF	Poly(vinylidene fluoride)
PMMA	Poly(methyl methacrylate)
PDMS	Poly(dimethylsiloxane)
AIE	Aggregation-induced emission
LED	Light-emitting diode

OLED	Organic light emitting diodes
RIM	Restriction of intramolecular motions
RIR	Restriction of intramolecular rotation
RIV	Restriction of intramolecular vibrations
TPE	Tetraphenylethene
THBA	10,10′,11,11′-tetrahydro-5,5′-bidibenzo[*a*,*d*] [7]annulenylidene
HPS	Hexaphenylsilole
AlQ_3	Aluminum tris(8-hydroxyquinoline)
DPDBF	Diphenyldibenzofulvene derivative
MA	Methylammonium
FA	Formamidinium
PLD	Pulsed laser deposition
SEM	Scanning electron microscope
VSM	Vibrating sample magnetometer
CIE	Commission Internationale de L'Eclairage
CCT	Correlated color temperature

S-R	Stretching-releasing
cpm	Cycles per minute
LAO	$LaAlO_3$
DPA-TPE	N,N-diphenyl-4-(1,2,2-triphenyl vinyl)aniline
$CHCl_3$	Chloroform
$CH_3NH_3PbI_3$	Methylammonium lead iodide
MAI	Methylammonium iodide
$PbCl_2$	Lead chlorine
DMF	N, Ndimethylformamide

Chapter 1 Introduction

Luminescence is the emission of light from an excited molecule. Luminescent materials, which also called phosphors, contain both inorganic and organic materials. The explore of novel luminesce materials and optical performances has been a major focus of research and development over the past decades, due to their wide applications in our daily life, ranging from solid-state lighting, architectural decoration, digital displays, to bio-imagines, optical sensors and lasers.

1.1 Luminescence and physical stimuli

1.1.1 Brief introduction of luminescence

Luminescence is referred to a phenomenon in which the electronic state of a substance is excited by external energy (photon, electron, etc.) and energy is released as light emission. Various types of luminescence may be distinguished by the method of excitation, such as photoluminescence (PL) arising from the absorption of photons,

electroluminescence (EL) by the application of an electric-field, and mechanoluminescence (ML) stimulated by mechanical stresses and so on.

Photoluminescence

PL is a process in which a substance absorbs photons (electromagnetic radiation) and subsequently radiates photons with light emission. This can be also described as an excitation to a higher energy state and then return to a lower energy state accompanied by the emission of a phono[1]. Generally, some PL emissions arise from dopant ions, which are known as luminescence centre or activator ion. Figure 1.1a shows the PL process. The electrons transition in the energy levels of the activator can better illuminate the mechanism of PL process. As Figure 1.1b shows, the excitation radiation is absorbed by the activator, raising it from the ground state to excited state. The electrons or excited ions return from the excited to the ground state by the emission of radiation. The energy difference between the excitation and emission is the internal energy transitions, which is released in the form of heat to the host lattice. Therefore, the emitted photon energy is typically lower than

absorbed. This redshift in emission spectrum is called the Stokes shift[2].

There are several possibilities for the electrons or excited ions returning to the ground state. The radiative transition generates light emission while the nonradiative transfer such as multiphonon relaxation and energy transfer between different ions cause energy loss in terms of heat. In the nonradiative transfer process, the energy of the excited state is used to excite the vibrations of the host lattice, i.e. to heat the host lattice. In order to create efficient luminescent materials, the nonradiative process needs to be suppressed.

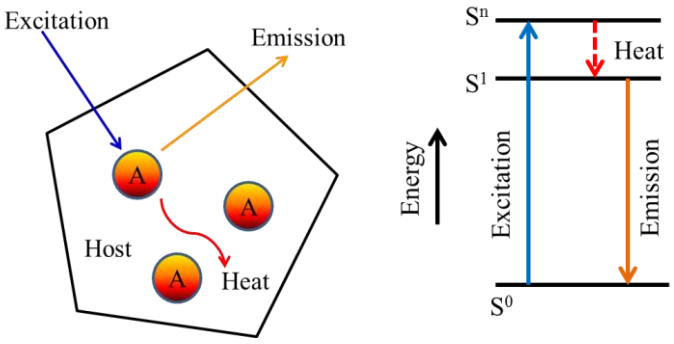

(a) (b)

Figure 1.1 (a) PL process with activators in the host lattice of luminescence materials. (b) Diagram of energy level of the PL process.

Luminescent materials are either semiconductors or insulators. The differences in the band gaps give rise to two mechanisms-band gap luminescence and characteristic luminescence, respectively. In the former case, luminescence occurs by electrons transiting from the conduction band to valence band. Sometimes, impurity ions are introduced to influence the luminescence properties, which are known as acceptor and donor ions. Acceptor levels located close to the valence band (eg., Cu^{2+} ion in $ZnS:Cu^{2+}$, Al^{3+}) can accept electrons, while donor levels located close to the conduction band can donate electrons (eg., Al^{3+} ion in $ZnS:Cu^{2+}$, Al^{3+})[3]. Characteristic luminescence arises by electrons transiting from higher energy to lower energy states at localized centres, for instance at the site of the activator ion.

Electroluminescence

EL is light emission from a substance under the excitation of an electric current or a strong electric field. EL phenomenon was first observed by Destriau in 1936 from the device based on ZnS phosphor powder dispersed in castor oil and sandwiched between two electrodes with a high AC voltage[4]. In 1968, Aron Vecht

first demonstrated a DC powered EL panel using powdered phosphor[5]. With the developing of transparent electrically conductive films of SnO_2, AC powder EL devices have been worldwide researched and developed. Mechanism involved in EL is the result of radiative recombination between electrons and holes. In briefly, electrons and holes may be excitation by high-energy electrons accelerated though a strong electric field. Subsequently, the electrons release their energy as photons when recombining with centers or positive holes accompanied by the light emission. The luminescence layer of EL device can be either inorganic or organic material. The typical inorganic phosphor used in thin-film EL (TFEL) is Mn^{2+} ion-doped ZnS particles with a yellow organic emission. Powdered ZnS doped with copper is the source of green light, while silver doped ZnS can produce bright blue light.

Mechanoluminescence

ML was first introduced into literature by Francis Bacon (1605), who observed a sparkling light from a hard sugar being nimbly scraped by a knife[6]. ML is defined as the phenomenon of light emission excited by mechanical action such as grinding,

cutting, friction, compression, stretching, and collision[7]. In some conditions, ML also called triboluminescence and piezoluminescence. However, triboluminescence differs from piezoluminescence in that a piezoluminescent material emits light when it is deformed, as opposed to broken (Figure 1.2).

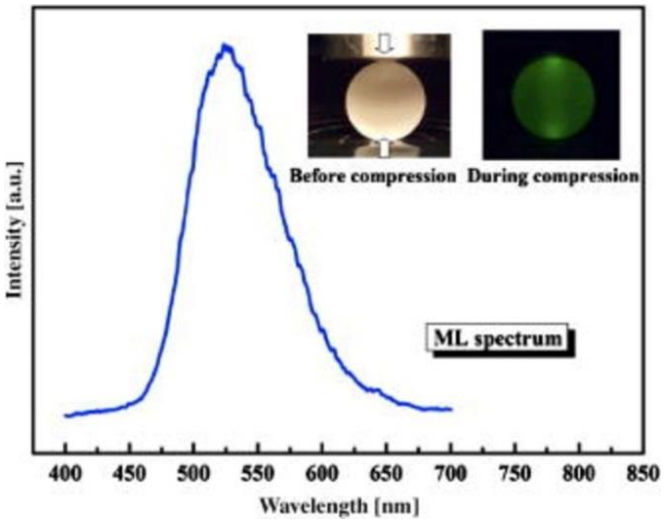

Figure 1.2 ML images and spectrum of green light from sample composed of ML ceramic powders and epoxy with a compressive stress[8].

In recent years, due to the research of intense ML observed in elastic ML materials, ML materials have made wide and important applications in remotely

mechanical stress detection in the form of visible light, pre-detection of sudden fractures in ceramic structures and forecasting earthquakes[9-11]. The most studied ML materials include rare earth doped strontium aluminates phosphors, metal ion-doped semiconductors (ZnS:Cu, Mn), and silicates. In these ML materials, the host often possesses non-centrosymmetric structure, which would give rise to piezoelectric potential in the inner crystal during elastic deformation; while the doped ion acts as the emitting centre. It is easy to understand the ML process by taking $CaZr(PO_4)_2:Eu^{2+}$ for example (Figure 1.3).

When stress applied on the ML phosphor, the deformation of $CaZr(PO_4)_2:Eu^{2+}$ crystal first builds in a local electric field in the inner crystal, and then the trapped electrons are de-trapped and excited to the conduction band (CB). Under a weak strain, only the electrons in shallower trap can be directly excited to CB. Electrons in the deep trap levels could be firstly excited to a shallower trap level and subsequently jumped to CB. The de-trapped electrons subsequently come back to the 5d levels of Eu^{2+}-h^+ and light emitted during the process of the de-excitation of

(Eu^{2+})* ions back to ground[12].

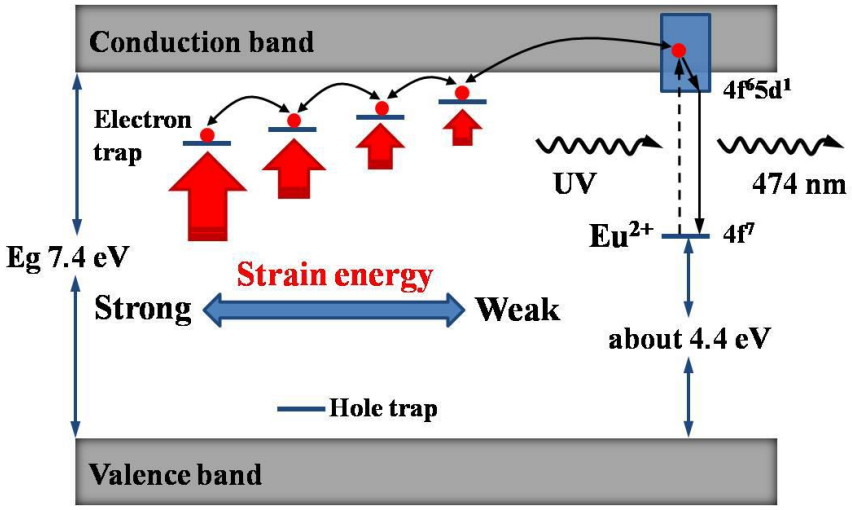

Figure 1.3 Schematic of ML process of $CaZr(PO_4)_2:Eu^{2+}$ phosphor[12].

1.1.2 Methods of physical stimuli

So far, tuning luminescence of phosphor materials has attracted widespread interest in various research fields, including optical sensing, information storage, and bioimaging. Conventional chemical way is focus on changing the chemical compositions, crystal structure, nanocrystal size, and so on[13]. These methods may suffer from the limitation of ex-situ and irreversible processes. Compared with the

chemical ways, the physical methods provide precise control over the process of modification luminescence properties by applying mechanical stress, magnetic field, electric field, temperature, ionizing radiation, and so on.

Mechanical stress

Due to the development of energy harvesting light sources, various mechanical stresses including friction, impact, compression, stretch and ultrasonic vibration are used in the research of phosphors which can stimulate the phosphors with light emission or tuning spectral properties. There is another kind of mechanical strain in which piezoelectric materials can response to applied electric field with piezoelectric strain, or magnetostrictive materials in response to external magnetic field with giant magnetostrictive strain. Utilizing these strains can precisely control the phosphors emission wavelength or intensity. Among the widely used piezoelectric materials, $Pb(Mg_{1/3}Nb_{2/3})_{0.7}Ti_{0.3}O_3$ (PMN-PT) single crystals is well known with its excellent piezoelectric coefficients (d_{33}>2000 pC/N) and high electromechanical coupling factors (k_{33}>0.9), which is capable of providing large biaxial strain due to the

converse piezoelectric effects. Recently, the luminescence of quantum-light-emitting diodes has been successfully tuned by the piezoelectric-induced strain from PMN-PT substrate[14] as Figure 1.4 shows.

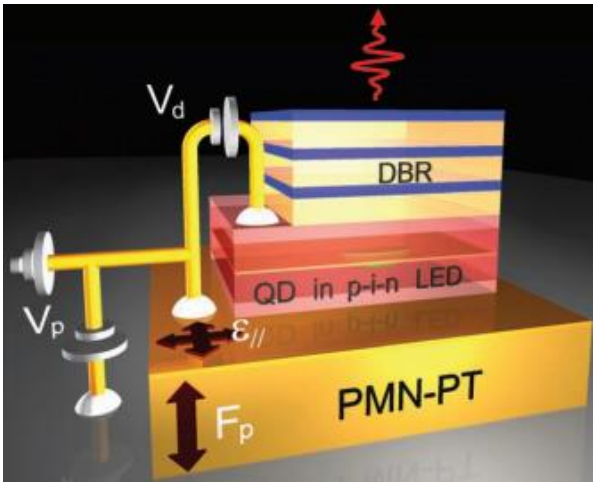

Figure 1.4 Schematic diagram of the strain-tunable single quantum dot resonant-cavity LED[14].

Electric field

To date, external electric field is typically used to tune the luminescence of phosphors due to the Stark effect, which is capable of splitting and shifting the spectral lines of atoms and molecules[15]. It is known that, electrons tend to shift to the anode and holes are pulled to the cathode under an external electric field.

Consequently, an electric-field-induced charge distribution may lead to an additional distortion of energy levels, resulting recombination efficiency modulation and emission peak shift. Additionally, due to the quantum-confined Stark effect[16], electric field can be used to tuning the luminescence of semiconductors nanostructures, such as quantum dots and quantum rods. It should be noted that dielectric hosts are commonly used in activator-doped phosphors, which can be polarized by an applied electric field, resulting to the change of the host symmetry and crystal field around the doped ions. This change can lead to luminescence manipulation of the dielectric phosphors.

Magnetic field

Optical-magnetic (OM) bifunctional materials are of great interest for developing advanced multifunctional devices. To achieve an OM interaction, a single-phase material should simultaneously have optical and magnetic properties to ensure the OM interaction occurs between atoms in the same crystal lattice, not at the interface between two separated phases with a high density of defects.

Luminescence tuning by a magnetic field is typically because of the Zeeman splitting of energy levels[13]. Take hexagonal-phase $NaGdF_4$ structure by lanthanide (Ln) doping for example, $NaGdF_4$: x%Nd^{3+}, 20%Yb^{3+}, 2%Er^{3+}. Magnetic tuning of the green emission is mainly due to the splitting of $^4S_{3/2}$ level into four Zeeman levels, | -3/2〉, | +3/2〉, | -1/2〉, and | +1/2〉, (Figure 1.5)[17]. An applied magnetic field decreases the total luminescent intensity from the $^4S_{3/2}$ quartet[18].

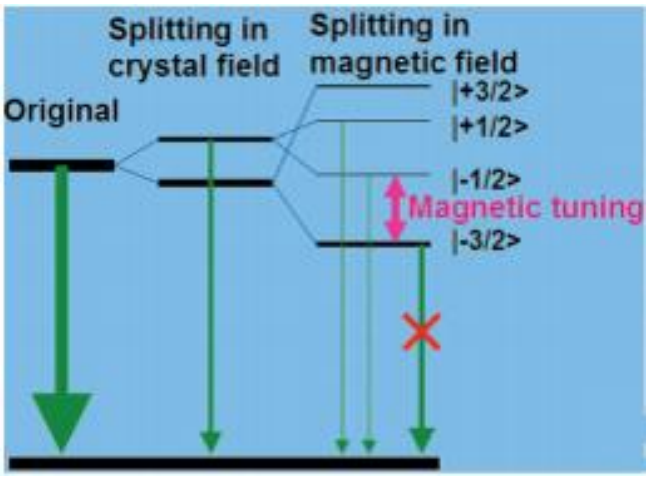

Figure 1.5 Schematic diagram of splitting of energy level $_4S^{3/2}$ of the Er^{3+} ion under external magnetic field[17].

1.2 Smart materials

Luminescence properties of smart materials have received increasing attention in the past few years due to their significant applications in photonic devices, optoelectronics devices and lasers.

Smart materials are designed materials with certain properties that can response to external stimuli (e.g., electric or magnetic field, mechanical stress, pH, and temperature)[19]. Various types of smart materials and their corresponding stimuli and representative materials are summarised in Table 1.1. Smart luminescent materials are designed materials which are capable of responding to external stimuli, such as stress, electric or magnetic field, resulting in intensity and/or color changes. In this work, smart luminescent materials chosen here are flexible phosphor composite, aggregation-induced emission (AIE) and organic-inorganic halide perovskite.

Table 1.1. 1 Common smart materials and its representatives.

Smart material types	Stimulus	Substance
Piezoelectric materials	Electric field or stress	PMN-PT, PZT, PVDF, $BaTi_3O_3$
Shape memory alloys	Temperature	NiTi, Fe-Mn-Si, Cu-Zn-Al
Magnetostrictive materials	Magnetic field	Terfenol-D, $Fe_{81}Si_{3.5}B_{13.5}C_2$
Polymers	Mechanical stress	PDMS, PMMA

1.2.1 Flexible polymer composites

Advances in micro and nanotechnology have motivated extensive studies on transparent and flexible polymer composites. These polymers have many advantages such as the flexibility, durable, optical transparency, easy fabrication, and compatible with arbitrary substrate characteristics. Functional materials in the size of micrometer or nanometer have been integrated into polymer matrix to form flexible polymer composites. Flexible polymers, such as poly(vinylidene fluoride) (PVDF), poly(methyl methacrylate) (PMMA), and poly(dimethylsiloxane) (PDMS) are widely used in electronics and phototronics materials and devices due to their compatibility and ease fabrication[20-22]. As a high-performance piezoelectric polymer, PVDF is was frequently integrated with good dielectric materials or magnetic materials to obtain better piezoelectric properties or magnetoelectricity, for example, PVDF packed with rare-earth-iron alloy $Tb_{1-x}Dy_xFe_2$ (Terfenol-D) and $PbZrTiO_3$ (PZT) exhibits a giant magnetoelectric (ME) effect[23]. PMMA usual mixed with pizoeletric materials to form thin film with excellent piezoelectric effect. PDMS is

the most widely used silicon-based organic polymer because it is optically clear and generally inert, nontoxic, and non-flammable. In addition, since it has low cost, ease fabrication, and biocompatibility, it is widely utilized in various microfluidic and nanogenerator applications. For example, ZnO nanowires and $BaTiO_3$ were mixed into PDMS to achieve good flexibility to be used on the surface of heart[24].

1.2.2 Piezoelectric single crystal PMN-PT

The piezoelectric effect was discovered in 1880 by Jacques and Pierre Curie[25].They found that the piezoelectric effect is a reversible process. In the direct piezoelectric effect, an applied stress on crystals, such as quartz, tourmaline, and topaz, induced an electrical charge on the crystal surface. Conversely, an electrical field applied on the crystal surface generate a mechanical strain. The piezoelectric effect is arose from the occurrence of electric dipole moments in non-centrosymmetric of solids crystal. Piezoelectric materials of complex perovskite type, such as PZT and PMN-PT have been attracting considerable attention for their high

piezoelectric performance. In contrast to PZT ceramics, PMN-PT single crystals show extraordinarily large electromechanical coupling coefficient, k_{33}>90%, and piezoelectric constant, d_{33}>2500 pC/N at room temperature[26-28]. Due to the mature Bridgman crystal growth method[29], PMN–PT crystals have been commercialized and continue to be an exciting research area in the promising applications of actuators, medical ultrasonic transducers and other electromechanical devices[10].

1.2.3 Aggregation-induced emission materials

AIE refers to a photophysical phenomenon characterized by a series of silole derivative materials that they are non-emissive when dissolved in good solvents as molecules but become highly luminescent when clustered in poor solvents or solid state as aggregate[19]. The AIE effect plays a constructive role in the luminescence process from luminogen aggregates, which may lead to hitherto impossible technological innovations[19]. The effect of AIE was first discovered in 2001 by Tang's group. Since then, many research groups have enthusiastically worked on the

mechanism and new structures of AIE materials, as well as relative applications. As a result, a large variety of AIEgens with emission color ranging from visible spectral to near infrared have been synthesized and widely used in optoelectronic materials, chemical sensors and biomedical probes[19,30-35].

The mechanism of AIE phenomena is the restriction of intramolecular motions (RIM)[19]. Molecular motions include rotations and vibrations. It is reported that the restriction of intramolecular rotation (RIR)[36] and restriction of intramolecular vibrations (RIV) are the main causes for the AIE phenomena observed in the propeller-shaped and shell-like luminogen system[37,38], respectively. Tetraphenylethene (TPE) is a well-studied AIEgen of the propeller-shaped system, while 10,10′,11,11′-tetrahydro-5,5′-bidibenzo[*a*,*d*][7]annulenylidene (THBA) is an emblematic the shell-like AIEgen luminogen system.

As Figure 1.6 shows, in TPE, four phenyl rings are linked to a central ethene rod and can rotate or twist against the ethane stator freely. In dilute solution, the intramolecular rotations of TPE molecules are activated, which lead to excited states

to the ground state in the form of non-radiatively decay. To the contrary, in the aggregate state of TPE, the intramolecular rotations are restricted and the radiative decays are activated, resulting in light emission enhancement[19]. On the other hand, the THBA molecule contains two flexible but non-coplanar parts and each part composes of two phenyl rings which are connected by a bendable flexure. These phenyl rings are able to dynamically bend or vibrate in the solution state due to the flexibility of the flexure, which activate the excited states to non-radiatively decay. Upon aggregate formation, the intramolecular vibrations become restricted due to the space limitation and physical constraint, which lead to the blocking of radiationless pathway and opening of the radiative decay channel, rendering THBA emissive in the aggregate state[19].

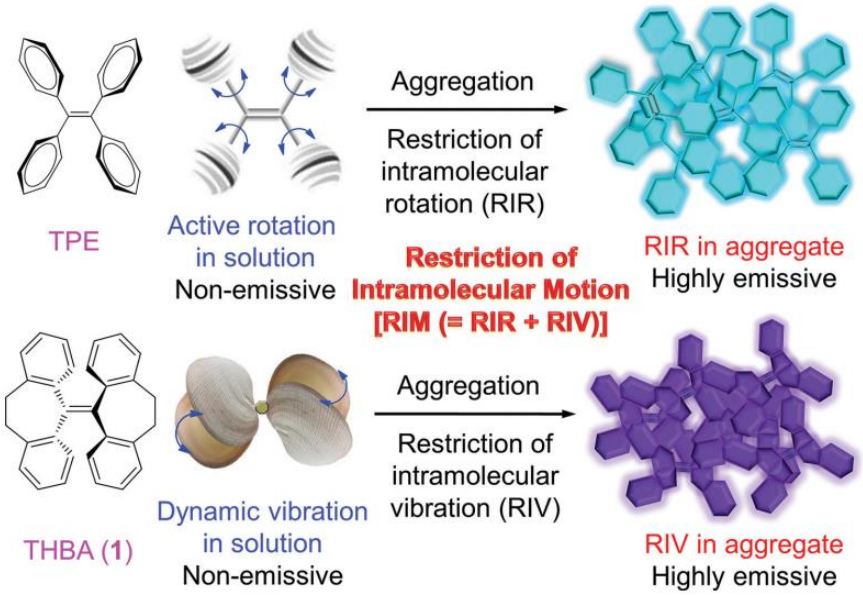

Figure 1.6 AIE phenomena arose from the restriction of intramolecular rotation (RIR) in the Propeller-shaped luminogen of tetraphenylethene (TPE). Shell-like luminogen of THBA (1) behaves similarly, due to the restriction of intramolecular vibration (RIV)[19].

1.2.4 Organic-inorganic halide perovskites

Organic-inorganic halide perovskites have attracted much attention in recent years due to its rapid advances in the performance of solution-processed photovoltaic technology[39-41].

The name of perovskite is original from the structure of $CaTiO_3$, which is discovered by Gustav Rose in 1839[42]. The family of perovskites share the same chemical formula ABX_3, where A is large bivalent cations (e.g., Ba^{2+}, Ca^{2+}, Sr^{2+} etc.), B is smaller tetravalent cations (e.g., Zr^{4+}, Ti^{4+} etc.), and X is anions, typically oxygen, halogens or alkali metals[42,43]. Notably, oxide-based perovskites have been the most widely studied of the perovskite family, due to its excellent ferroelectric, piezoelectric, magnetoresistive and superconductive properties. Organic-inorganic halide perovskites are different from the inorganic oxide counterparts with monovalent organic moieties occupy the A-site (e.g., $CH_3NH_3^+$, $HC(NH_2)_2^+$ etc.), divalent metal cations at B-site (e.g., Pb^{2+}, Sn^{2+}, Ge^{2+} etc.), and halides at the X-site (e.g. Cl^-, Br^-, I^-). Similar to the inorganic oxide perovskite, halide perovskites must obey allowable tolerance factors to achieve the crystal symmetry. Figure 1.7 shows a distinction between the structures of organic and inorganic perovskites. It is obviously that the A-site ion is different, Cs^+ is inorganic and $CH_3NH_3^+$ is organic. Aside from that, a change in symmetry of the A site component from spherical

(inorganic) to non-spherical (organic) must be noted, which will lead to distinction in term of orientational disorder and polarization[44,45].

The exceptional properties, including high carrier mobility ((in excess of 10 cm^2 V^{-1} s^{-1})[46], long diffusion lengths (up to 1 μm or even beyond)[47,48], low trap density (less than 10^{16} cm^{-3})[49], minimal stokes shift (less than 20 meV)[47], and an adjustable spectral absorption range make it advance in the applications of solar cells, lasers, LEDs, photodetectors, and more.

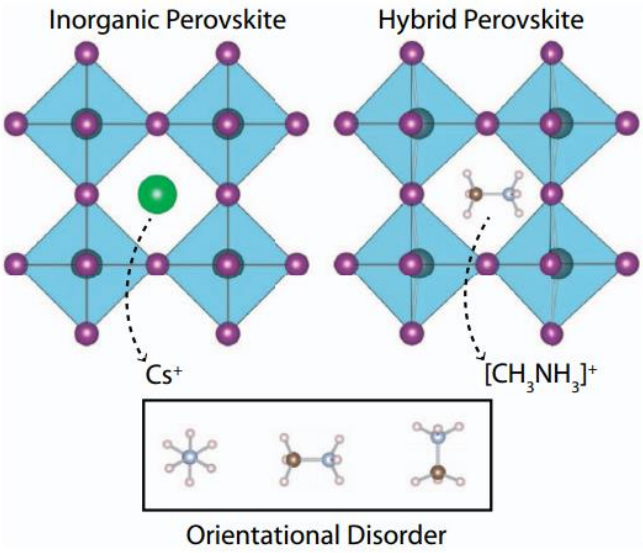

Figure 1.7 Orientational disorder associated with the nonspherically symmetric organic CH_3NH^{3+} cation versus the spherically symmetric inorganic Cs^+ cation[45].

By tuning the halide composition of the perovskite, its bandgap can be tunable, allowing the PL spectrum varies from visible to near-infrared wavelengths[50]. LEDs based on the halide-substituted $CH_3NH_3PbX_3$ family, as well as inorganic $CsPbBr_3$ were recently reported with high external quantum efficiencies and current efficiency[51,52]. In addition to thin film based LEDs, bright emission was also observed from nanostructured perovskites[53,54]. The method for tuning the photophysical properties of perovskites via ions substitutions, as well as size and morpholopy manipulation amount to a broad palette of potential for light-emitting devices.

1.3 Literature review

1.3.1 Advance of mechanoluminescence

ML material is a kind of phosphor that capable of converting mechanical stress into light emission. Though ML emission was first reported to be discovered in the breaking sugar crystals in 1605, research into ML materials primarily originates from

the last few decades because of the weak and unrepeatable properties of some ML materials[7]. Much effort has been devoted to find more intense and repeatable elastic ML phosphor materials. Up to now, a series of elastico-mechanoluminescence (EML) phosphor materials with different emission colors by doping rare-earth-ions into silicates, titanates, aluminates, as well as zinc sulphide. The most commonly used ML phosphors are listed in Table 1.2. Interestingly, all ML phosphors show similar ML, PL and EL emission spectra as they originate from the same dopant ions. These phosphor materials can be synthesized in several forms, including particle, thin film, ceramic disk, pellet, and composite.

Table 1.1.2 Typical EML phosphor materials[55].

Host	Dopant	ML (nm)	PL (nm)	EL (nm)	Ref.
$SrAl_2O_4$	Eu^{2+}, Eu^{2+}/Dy^{3+}	524	524	524	[11,56,57]
	Ce^{3+}, Ce^{3+}/Ho^{3+}	300-500	300-500	-	[58]
	Eu^{2+}/Er^{3+}	524,1530	524,1530	-	[59]
ZnS	Mn^{2+}	580	580	580	[9,60]
	Cu^{2+}	517	517	517	[61]
	Mn^{2+}/Cu^{2+}	587	587	587	[60]

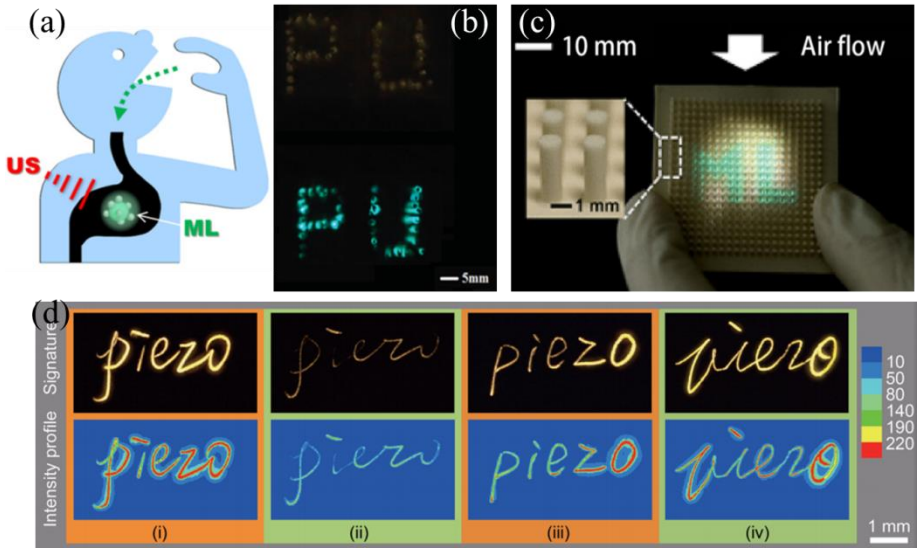

Figure 1.8 (a) Schematic illustration of ML phosphors being used in bioimaging and phototherapy[62]. (b) Display of green colored logo “PU” from ML materials without (upper) and with magnetic field (lower)[63]. (c) Display of patterned ML device driven by a wind[6(a) Schematic illustration of ML phosphors being used in bioimaging and phototherapy[62]. (c) Display of patterned ML device driven by a wind[64]. (d) Demonstrations of recording the signing habits with an ML-based device: pressure evenly distributed during signing process with strong force (i) and weak force (ii); more pressures applied at the end (iii) and some turning points (iv) of the signing process[65].

The ML phosphors are capable of converting mechanical energy into light emission. Their characteristics of sensing various mechanical stresses have shown the potential applications in stress sensor, optical imaging, artificial skin, and structural health diagnosis and so on[58,62]. Terasaki first proposed the concept of using the ML phosphor in bioimaging and phototherapy[62,66]. Figure 1.8a shows the schematic that light emits from the ML phosphor excited by ultrasonic wave. In comparison with labeling techniques based on PL, this method is noninvasive and nondestructive, avoiding the photo damage and excitation radiation to tissues[55]. Notably, a potential application for ML materials is display (Figure 1.8b and c). Our group has previously demonstrated the display of green colored logo “PU” representing the abbreviation of the Hong Kong Polytechnic University from ML magnetic phosphor composite under the stimulation of low magnetic field[63]. Very recently, Jeong et al. presented the color manipulation by controlling the weight ratio of two different ML materials emitting orange and green colors in a soft polymer matrix under mechanical stress stimulation[60]. The color region can also be tuned by

varying stress rate. Furthermore, a wind-driven ML system consisted of phosphor particles embedded in an elastomer has been demonstrated. The interesting results imply a potential use in harvesting wind power for illumination[64], although the gas flow simulated as wind requires a speed of 40-100 m/s which is within the range of hurricane or typhoon and therefore further improvement is needed to suit for more accessible mechanical stimulus. Intriguingly, Pan et al. integrated the metal ion-doped ZnS ML phosphor with PDMS into a high sensitive piezoelectric composite to collect electronic signatures[65], shown in Figure 1.8d. Compared to the typically handwriting graphics, the ML-based system providing a higher level of security as it contains both the signature graphics and the signing habits (e.g., pressure applied on each character) of the signees.

1.3.2 Mechanochromic properties of AIE materials

Mechanochromic material is a kind of smart material whose emission color or intensity can be changed in response to mechanical stimuli such as grinding,

pressing, rubbing or crushing[67-71]. The mechanochromic property of smart materials is of significance for their promising applications in optical storage, mechanosensors, and security papers and so on[72-74]. To date, lots of AIEgens possess irreversible mechanochromic luminescence have been synthesized[19,69,75]. The mechanochromic property of AIEgens was first observed in crystal of hexaphenylsilole (HPS) which is a typical AIEgen and has crystallization-enhanced emission effect[76,77]. When a hydrostatic pressure was applied to the amorphous HPS thin film, its PL intensity became stronger as Figure 1.9a shows[77]. The Aluminum tris(8-hydroxyquinoline) (AlO_3) thin film shown in Figure 1.9b was used as reference whose PL intensity is monotonously decreased with increasing pressure. The reason for the increased PL intensity under low hydrostatic pressure may be that the stronger intermolecular interaction induced by pressure restricts the aromatic rings.

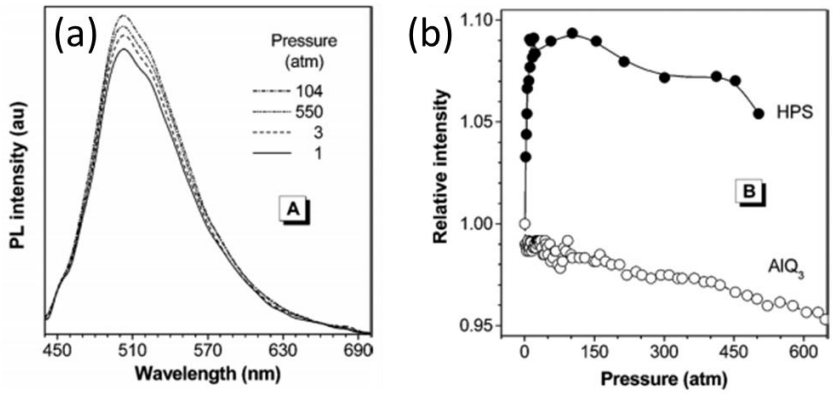

Figure 1.9 (a) PL spectra of HPS thin film at different pressures and (b) PL intensity of HPS and AlQ_3 films under pressure[77].

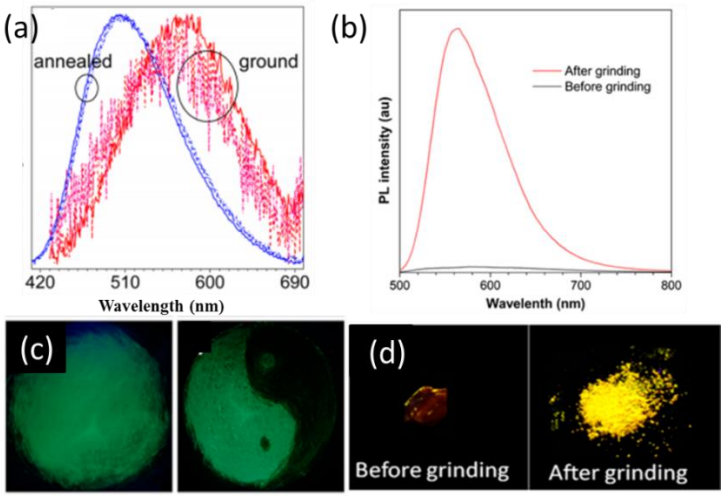

Figure 1.10 PL spectra and photos of luminogens (a) DPDBF derivative and (b) MC-active before and after grinding[78,79].

In addition to static pressure, the grinding stress may cause color emission change. Figure 1.10 shows two types of AIEgens with mechanochromic property. The crystal of a diphenyldibenzofulvene derivative (DPDBF) emits bright green light before grinding (Figure 1.10a and c). After grinding, the PL of DPDBF becomes weaken and re-shift to orange color. This color transform suggests that the crystals are amorphorized upon grinding[78]. Like DPDBF derivative, many AIEgens show a weaken emission intensity under mechanical stress. Intriguingly, Jia constructed a luminogen with dipeptide and pyrene, which demonstrates "turn-on" mechanochromic luminescence due to different excited states in the amorphous and crystalline states[80]. Figure 1.10b and d show a type of mechanochromic active AIEgen, which emits a strong PL at 563 nm with a high quantum yield of 48% after grinding or hitting[79].

The color contrast of many AIEgens with mechanochromic emission is low. Recently, two AIEgens with high color contrast are synthesized by attaching a pyridinium[81] or benzothiazolium[82] unit to TPE. After grinding, they transform to

amorphous powders with a red-shift in color and a high emission contrast of ca. 85 nm. Due to the loosely packing planar structure of AIEgens, their transformation between different morphologies can be realized by mechanical stimuli, heating and solvent fuming[83] (Figure 1.11).

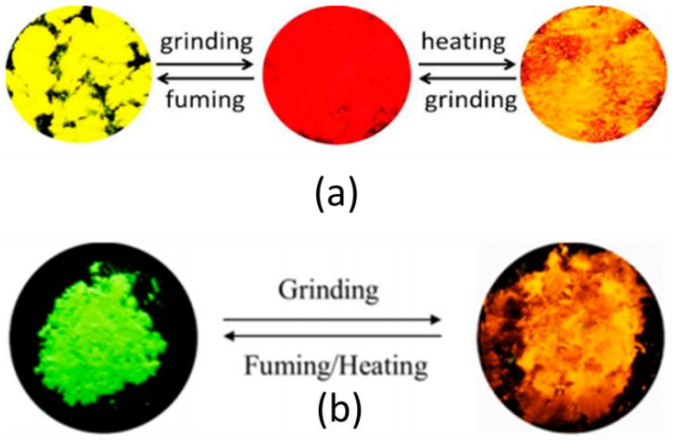

Figure 1.11 Emission color switching of (a) **12** and (b) **13** among the processes of grinding, fuming and heating[82,81].

1.3.3 PL tuning of organic-inorganic halide perovskites

Recently, organic-inorganic halide perovskites have been emerged in

optoelectronics[84,85], for its remarkable performance in solar cells with high power conversion efficiencies (PCE) of 20%[86]. Thin films based on perovskites also demonstrate high photoluminescence quantum yield (PLQY)[87], which led to the development of LEDs and lasers[88,89].

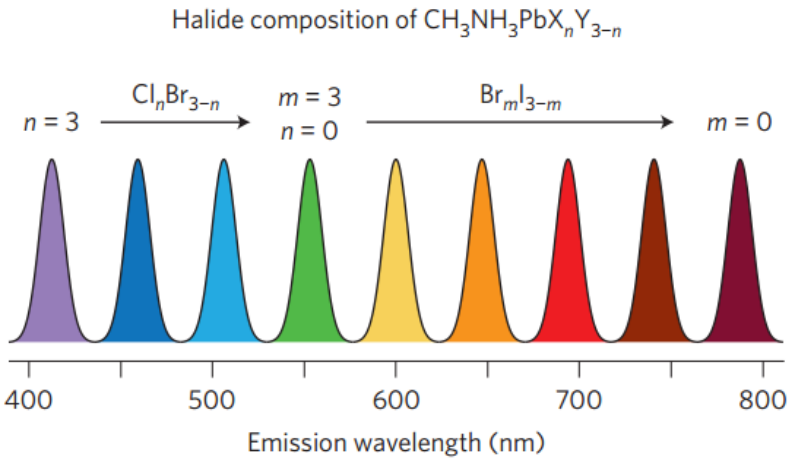

Figure 1.12 Emission wavelength tuning of $CH_3NH_3PbX_nY_{3-n}$ perovskite materials[90].

Perovskites possess the crystal structure ABX_3, where A is $CH_3NH_3^+$, Cs^+, $CH(NH_2)^{2+}$ cation, B is Pb^{2+} or Sn^{2+} and X is typically Cl^-, Br^-, I^- anions[90]. The PL spectrum and other optoelectronic properties of ABX_3-type perovskites can be tuned

by varying the organic cation, the metal ions and the halide anions or doping other ions[89,91,92]. For instance, Methylammonium (MA) lead trihalide perovskites have the chemical composition $CH_3NH_3PbX_nY_{3-n}$, whose PL emission spectra can be tunable ranges from 390 to 790 nm (Figure 1.12) by cation substitution or blending[90]. In addition, the emission wavelength is extended to 820 nm through mixed MA with formamidinium (FA)[93]. The lead-free perovskites based on $MASnX_3$ have an emission wavelength to 900 nm[94], which represents the promising of environmental friendly optoelectronic devices. These chemical techniques to modification the PL spectrum of perovskites is of significance for their applications in LEDs, lasers and solar cells.

Contrast to the extensively reported chemical methods, physical techniques used to tune the PL of perovskites has limited report. Up to now, only the hydrostatic pressure has been reported to tune the bandgap and PL emission properties of the $MAPbX_3$ single crystals[95,96].

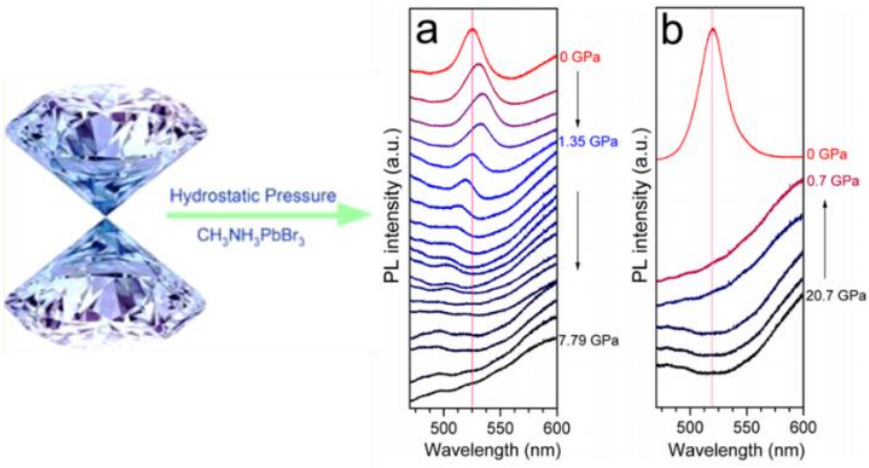

Figure 1.13 PL spectra of $MAPbBr_3$ single crystal as a function of pressure during (a) compression and (b) decompression [95].

As Figure 1.13 shows, an anomalous PL emission peak shift from the $MAPbBr_3$ single crystal was observed during the pressure varying from 1 to 5 GPa[95]. Phase transition occurs between amorphization and orthorhombic structure. Similarly, a significant PL peak shift and intensity change was observed from the $MAPbI_3$ single crystal during the pressure varies from 0 to 5.3 GPa (Figure 1.14)[96]. It is notable that tuning of PL spectra of $MAPbX_3$ perovskites by pressure is almost reversible. In addition to hydrostatic pressure, small isotropic stain of -2% has been calculated to

be able to cause an increase of band gaps of the Sn-containing perovskite such as $CH_3NH_3SnI_3$ and $CsSnI_3$[97].

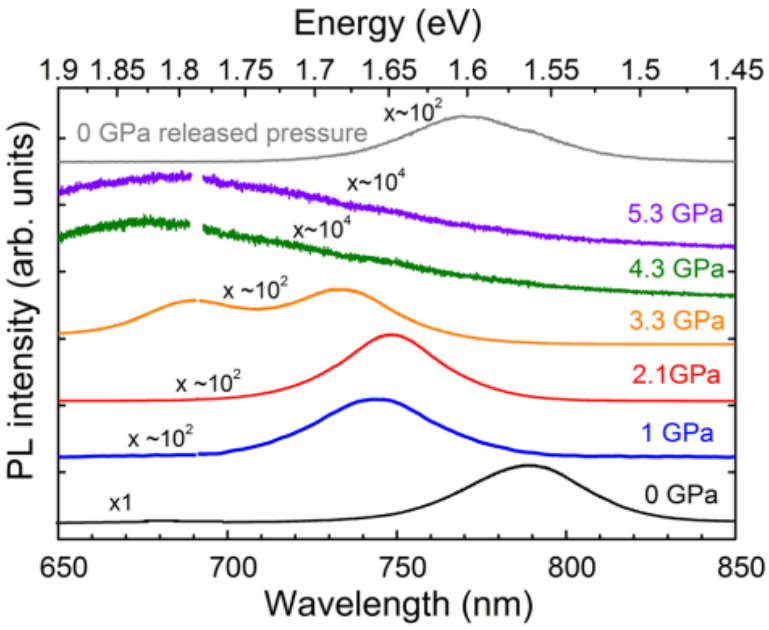

Figure 1.14 PL spectra of $MAPbI_3$ single crystal under pressure[96].

1.4 Motivation of this thesis

Energy-saving solid-state lighting based on light-emitting diode (LED) has increasingly been used in our daily life, such as general illumination and backlight for liquid-crystal display[98,99]. Currently, white light is typically obtained from an

InGaN blue LED integrated with a phosphor (e.g., YAG: Ce) layer, which consists of p-n junction based blue LED and are rigid in nature. Therefore, it is fascinating to explore new strategies with the configurations beyond the p-n junction based structure, as well as the light sources with flexible feature which can be triggered by multiple stimuli, such as electric field and various mechanical stresses.

Compared with enormously studied PL and EL, ML has great potential as light sources and displays for its capability of converting mechanical energy into light emission[64,100]. According to the piezo-phototronic effect[101], when a strain is applied to a piezoelectric semiconductor, the charge transport behavior can be tuned, resulting in improving the performance of optoelectronic devices[102]. Inspired by this idea, we have previously reported the piezo-phototronic effect-induced dual-mode orange light and ultrasound emissions from ZnS:Mn thin film grown on piezoelectric PMN-PT substrate[103]. However, the reported thin-film structure fabricated by pulsed laser deposition (PLD) is rigid, which limits the wide application of ZnS based phosphors. Therefore, a kind of flexible composite of metal ion-doped ZnS mixed to

PDMS matrix has been prepared which features flexible, durable, easy, and cost-effective fabrication with no use of vacuum, and compatible with almost any type of substrate. With these merits of the composite phosphors, light-emitting device from the composite phosphor-based hybrid structures free of p-n junction has been fabricated.

On the other hand, developing smart phosphor materials with tunable light emission has always been attractive at the forefront of color display, optical sensing and information storage[104,105]. Currently, the extensively studied conventional chemical approaches used to tuning the luminescence of phosphors have focused on the phosphor's synthesizing process. Obviously, the chemical method is an irreversible and the kinetic process of luminescence changes with the crystal field and structural symmetry is unclear. Thus, it is significant to broaden the modulation of luminescence by physical methods, such as electric field[106], magnetic field[17] and mechanical stress[107]. Note that some of the AIE materials are capable of changing colors under grinding. Thus, it is interesting to study the effect of electric field or

magnetic field tuning the AIE emission in terms of strain. Interestingly, the new favorite organic-inorganic halide perovskite is deduced to be ferroelectrics, which is considering to be excellent optoelectronic materials for its remarkable spectral absorption range and long diffusion lengths[87,108,109]. Besides, environment factors such as oxygen, temperature, and humidity have significant influence on the PL spectrum and efficiency of photovoltaic devices[110-112]. Thus, it is essential and interesting to tuning the PL spectrum of organic-inorganic halide perovskite material by strain.

1.5 Objective and structure of this thesis

The main objectives of the present research are summarized as follows: the first one is to investigate light emission from flexible polymer composite excited by multiple mechanical stimuli, such as uniaxial strains of stretch and mechanical writing, and piezoelectric biaxial strain. The optical characteristics of CIE, luminance, and CCT have also been investigated under different mechanical strain.

The second one is to explore a new approach to modulate the AIE PL emission by the mean of piezoelectric strain induced by PMN-PT substrate with external ac electric field. In addition, magnetic compress strain also utilized to tune the AIE PL emission. The last one is trying to enhance and modulate the PL emission from organic-inorganic perovskite thin film with the piezoelectric substrate.

The thesis consists of six chapters. Introduction in chapter 1 gives an overview of three types of luminescence (PL, EL, and ML), multiple stimuli, and smart materials. In addition, the relevant physics of luminescence and properties of smart materials were including in chapter 1.

Chapter 2 describes the sample fabrication techniques and characterization methods used in the thesis.

In Chapter 3, bright white light was obtained from the flexible polymer composite consisted of metal ions-doped ZnS phosphor and PDMS matrix under the excitation of uniaxial stress of stretch and release. A piezoelectric optoelectronic device was fabricated and characterized based on the piezoelectric strain induced

luminescence. The relationship between luminescence intensity and strain has been investigated.

Chapter 4 presents two different ways to modulate the PL emission from AIE thin film. Piezoelectric strain and magnetostrictive strain were first used to modulate the luminescence of AIE thin film.

Chapter 5 demonstrates the piezoelectric strain tuning PL emission from organic-inorganic perovskite thin film coated on the PMN-PT substrate.

Chapter 6 gives the conclusions and suggestions for future work.

Chapter 2 Experimental Techniques

All the phosphor thin film layers studied in this thesis were prepared by spin coating method. Electrodes used for the luminescent devices in this thesis were fabricated by sputtering. The structures of thin films and device were determined by scanning electron microscope. The magnetization property of the Fe-Co-Ni magnetic phosphor composites was characterized by vibrating sample magnetometer. The luminescent properties of these phosphor composites and luminescent devices were investigated by fluorescence spectrometer.

2.1 Device preparation

2.1.1 Spin coating

Spin coating is a facility method to form uniform thin films on a flat substrate. It is used for coating in organic electronics, optical devices, microelectronics industry, and magnetic storage disks.

A typical procedure flow diagram is described in Figure 2.1. A small amount of

fluid materials is dropped onto the center of a substrate. The substrate is then rotating at a high speed (typically around 3000 rpm), which generates a centrifugal force to spread the coating material to become an even coating. After the solvent evaporates, a layer of thin film leaves on the substrate. Sometimes, a separate drying step is needed at center temperature to further dry the film.

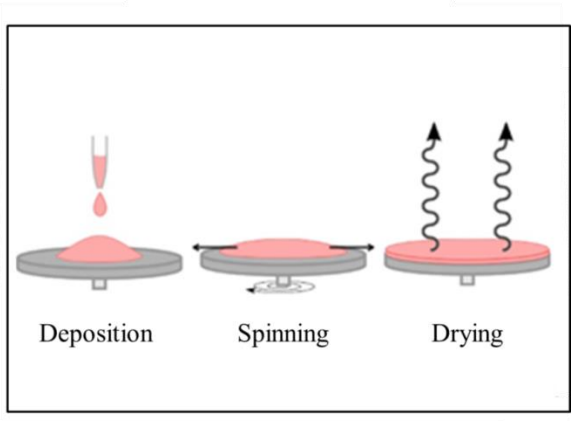

Figure 2.1 Diagram of the procedure of spin coating.

Generally, the thickness of a spin coated film is proportional to the inverse of the spin speed squared. The exact thickness of a film will depend upon the coating materials such as viscosity, concentration, drying rate, and surface tension as well as the parameters chosen for the spin process (rotation speed, time, and fume exhaust).

Therefore, the spin thickness curves for certain materials are most commonly determined empirically.

The mainly advantage of spin coating is its easy and fast fabrication of uniform films with thickness ranges from nanometres to microns. The disadvantage is its relatively low throughput compared to roll-to-roll processes as well as faster drying time which leads to lower performance for self-assemble and crystallize process.

2.1.2 Magnetron sputtering

Magnetron sputtering is a type of physical vapor deposition (PVD), a process in which a target material is vaporized and deposited on a substrate to form a thin film. Generally, a sputtering process begins in a vacuum chamber with the target material place in the cathode side as shown in Figure 2.2. Energetic electrons firstly bombard the inert gas such as argon atoms and knock off the electrons in their outer electron shells. As a result, the positive argon ions (Ar^+) are accelerated to the target by the electric field. The forcefully collisions lead to the target atoms ejects into space. The

ejected atoms then travel some distance until the reach the substrate and condense into a thin film. During the process, a magnet is introduced to stabilize the free electrons. The magnetic field keeps the electrons traveling spiral along magnetic flux lines near the target instead of being attracted toward the substrate. Since the magnetic field lines are curved, the path of the electrons in the chamber is extended through the stream of argon. In this way, magnetron sputtering offers higher ionization probability and shorter deposition time, as well as less electron damage to the target material than traditional sputter deposition techniques.

Sputtering is one of the most common ways to fabricate thin films due to its easy deposition of high melting points materials, no decomposition of metallic target, and compatible with reactive gases such as oxygen. The film deposited by magneton sputtering is characterized with high smooth, excellent layer uniformity, and close to the composition of the source material. Compared to the evaporation, films deposited by sputtering have a better adhesion on the substrate.

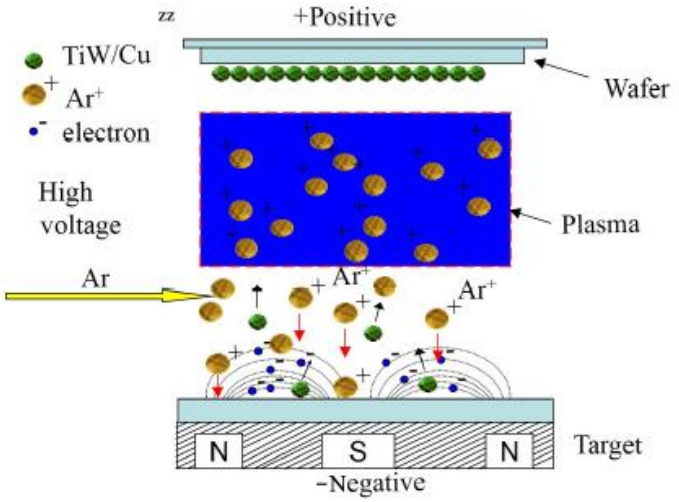

Figure 2.2 Schematic diagram of magnetron sputtering process[113].

2.2 Characterization

2.2.1 Scanning electron microscope

Scanning electron microscope (SEM) is a kind of microscope that uses a focused beam of electrons to image the surface of a sample. Photo of the SEM equipment used in the laboratory is shown in Figure 2.3. The incident electron beam is scattered in the sample and gives rise to various signals that contain information of surface topography and composition of the sample. The high-energy electron beam

shot from electron gun, travels through the grid static electric field, electromagnetic field and lens, and then focuses to be a smaller electron beam to scan the sample. As a result, various signals excite from the sample including secondary electrons, backscattered electrons, photons of characteristic X-ray and cathodoluminescence and transmitted electrons.

Figure 2.3 Photograph of SEM.

These signals come from various depths of the sample as Figure 2.4 shows. The secondary electrons generated close to the surface that show the topographic information of the sample. The typical measurement mode of SEM is the detection

of secondary electrons image which has high resolution signals with a resolution of 1~2 nm. The backscattered electrons are emerged by elastic scattering within the deeper locations of the sample so that they have a poorer resolution compared to the secondary electron images. As the intensity of the backscattered electrons image is determined by the average atomic number (Z) of the sample, backscattered electrons image is often used along with the characteristic X-rays spectra in analytical SEM.

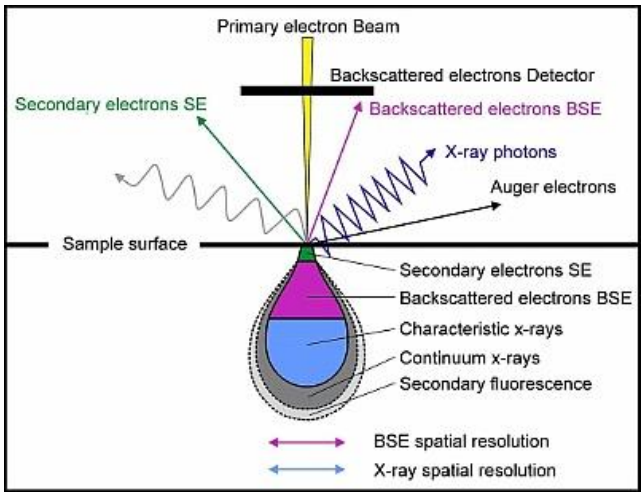

Figure 2.4 Schematic diagram of interactions between electrons and the sample[114].

Backscattered electrons images illustrate the distribution of different elements

in the specimen. The characteristic X-rays are photons not electrons. Therefore, they have poor spatial resolution than secondary electrons and backscattered electrons. The detection of X-ray signals need longer recording time due to its relatively few emitted and the inefficient detector. Generally, the information of the composition and abundance of elements is obtained by detecting the characteristic X-rays.

For traditional SEM image, samples must be electrically conductive. Consequently, insulating samples are usually coated with an ultrathin layer of electrically conducting material. With the introduction of environmental SEM (ESEM), insulating samples can be imaged without coating. Besides, some other challenging samples can also be imaged by ESEM, such as biological samples which are vacuum sensitive, irradiation sensitive samples like thin organic films, and oil samples. The ESEM can be used to study and image chemical and physical processes in-situ, such as mechanical stress testing, oxidation of metals, and hydration. ESEM has significantly simplified the imaging of challenging samples.

2.2.2 Vibrating sample magnetometer

The vibrating sample magnetometer (VSM) is utilized to test the magnetic properties of sample. The VSM was invented by Simon Foner at Lincoln Laboratory MIT in 1955. The VSM used in our laboratory was provided by the LakeShore 7407 system (shown in Figure 2.5) which has the ability to characterize the DC magnetic properties of materials as a function of magnetic field, time and temperature. The VSM provides a static magnetic field that can reach up to 3.42 T and a broad temperature range from 4.2 K to 1273 K. Consequently, a wide range of materials can be measured.

During the VSM testing, the sample is placed in a uniform magnetic field to be magnetization. Then it is vibrated sinusoidal along z axial direction through a piezoelectric material actuator. As a result, the magnetic flux through a nearby pickup coil varies sinusoidally. The induced voltage is proportional to the sample's magnetic moment but independent on the applied magnetic field, which is measured by a lock-in amplifier. Therefore, the magnetic hysteresis curve of the sample is

obtained by measuring the ac electric signal.

Figure 2.5 VSM system used in our laboratory.

2.3 Optical spectroscopy

2.3.1 Photoluminescence spectrometer

PL spectrometer is used to measure the luminescent properties in the ultraviolet-near infrared spectra range. The PL spectrometer can be used to conduct steady-state and time-resolved measurements. The steady-state PL analysis can measure both excitation and emission spectra of samples. An excitation spectrum is measured at a single emission wavelength while an emission spectrum is the wavelength distribution of photons emitted by molecules or atoms measured at a

single constant excitation wavelength.

In the time-resolved PL test, a pulse light source is used to excited the sample and the decay in PL is recorded with respect to time. The time-resolved PL spectrum is helpful for measuring the lifetime of minority carrier. PL decay kinetics gives a complete image of the phosphor and its interactions within the microenvironment, which is benefit for researchers gaining a deep understanding of the electronic structure and reaction mechanisms of the phosphor materials. Consequently, time-resolved PL is broadly used in the research of physics, chemistry, and biology.

Two kinds of spectrometers are used in our laboratory. The most commonly used is Edinburgh FLSP920 spectrometer which can characterize both the steady-state and time-resolved PL. Samples including Powder, thin film and liquid samples can be measured using different quartz sample holders. The picture of FLSP920 spectrometer is shown in Figure 2.6.

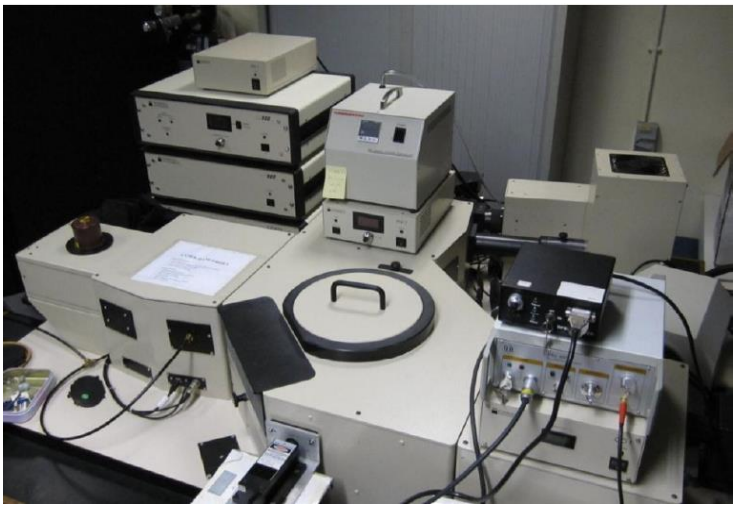

Figure 2.6 Picture of Edinburgh FLSP920 spectrometer.

Edinburgh FLSP920 spectrometer systems mainly include light sources, grating, detectors, and computer controller. Each individual functional component (Figure 2.7) is described as follow.

Excitation light sources: The FLS920 comes standard with a xenon arc lamp, and a variety of other sources can be integrated such as microsecond and nanosecond flashlamp, pulsed diode lasers, pulsed light emitting diodes, infrared continuous wave (CW) and pulsed lasers. Xe900 Xenon Arc Lamp is a 450 W ozone free xenon arc lamp that covers a wide range of 230 to 1000 nm for the steady-state PL

measurements. Continuous 980 nm Laser diode is used as an excitation source for NIR or upconversion PL measurement. μF900 Microsecond Flashlamp can generate short and high irradiance optical pulses at repetition rates up to 100 Hz. nF900 Nanosecond Flashlamp can provide sub-nanosecond pulses over the spectra range from 110 to 850 nm at repetition rates to 100 kHz. Both μF900 and nF900 Flashlamps can be used as excitation source in the time-resolved PL measurement.

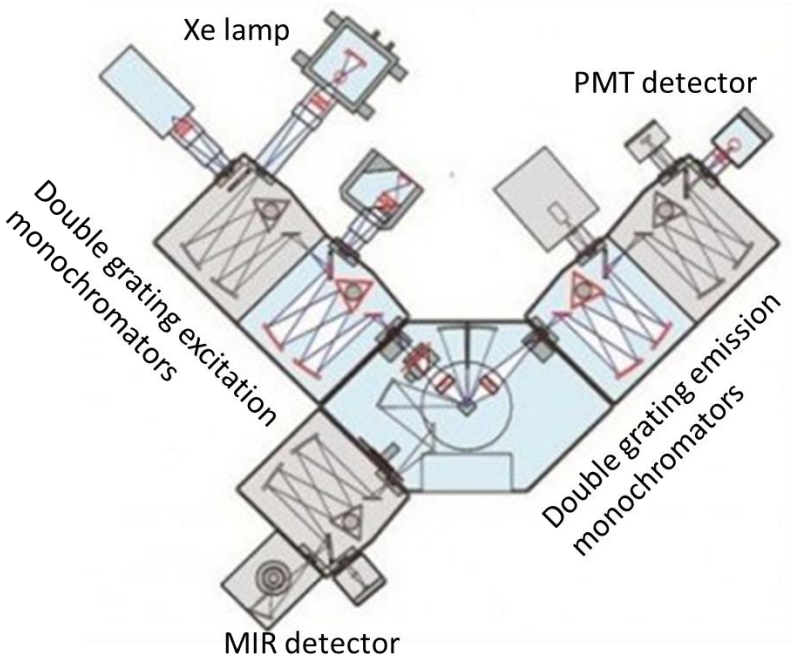

Figure 2.7 Schematic diagram of Edinburgh FLSP920 spectrometer.

Grating: Single and double grating Czerny-Turner monochromators are available in the FLS920 with 300 mm (or 2 x 300 mm) focal length, 250/500 nm blaze, 1800 grooves/mm, 0.05-18nm resolution and 0.2 nm wavelength accuracy. They have excellent properties, such as great stray light rejection, low temporal dispersion, and high optical throughput.

Detectors: The FLS920 comes standard with two types of detectors. Red sensitive Photomultiplier (PMT) is available spanning the range from 185 nm to 850 nm at -20 °C. NIR PMT operated at -80 °C can respond to the spectral range from 300 nm to 1700 nm.

The other kind of spectrometer is USB4000 Fiber Optic Spectrometer produced by Ocean Optical incorporated. The steady state PL measurement by USB4000 covers a range of 200 to 1100 nm. Its 3648-element CCD array detector and powerful high-speed electronics provide a high optical resolution up to 0.1-10 nm FWHM and fast spectral response with the integration time of 3.8 ms-10 seconds. The fiber optical based spectrometer of USB4000 is characterized with portable and

compatible that it can directly bring to the sample and easily integrated as an OEM component.

2.3.2 Spectroradiometer

A spectroradiometer is a device designed to measure the spectral power distribution of a light source. The spectral power distribution of a source expresses the per-wavelength contribution to the radiometric quantity. In other words, the spectroradiometer detects the light, then separates each wavelength and takes an individual reading for each color.

The spectroradiometer at our laboratory is PR-670 from Photo Research Inc. Spectroradiometers typically take measurements of spectral irradiance and spectral radiance. Following a measurement, the PR-670, displays data and color spectral graphs on the system display. It is a useful tool to detect the color characteristics such as Commission Internationale de L'Eclairage (CIE) coordinates, luminance and correlated color temperature (CCT), illuminance, and dominant wavelength. Figure

2.8 shows the C.I.E. 1931 Chromaticity Diagram, providing a visual representation of the color properties of a light source. The CIE, CCT and luminance can be directly read from the measurement results while the luminosity can then be calculated through mathematical integration. These metrics are significant for evaluating the ability to render colors of a light source.

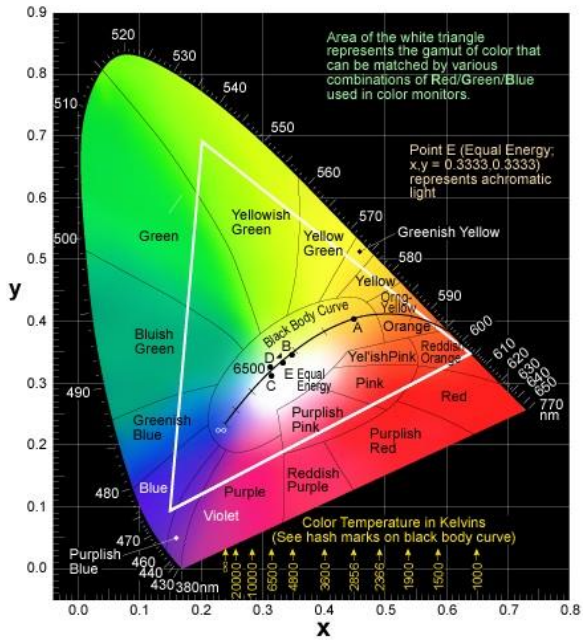

Figure 2.8 C.I.E. 1931 Chromaticity Diagram.

The PR-670 has a unique, portable and versatile design as its operating

parameters shown in Table 2.1. This makes tasks such as spectrally based photometric and colorimetric measurements, and source spectral power distribution quick and simple.

Table 2.1 Operating parameters of Spectroradiometer PR670.

Detector	256 Detector Array
Spectral range	380-780 nm
Spectral Resolution	1.56 nm / pixel
Spectral bandwidth	8 nm (5 nm optional)
Spectral Accuracy	± 1 nm
Luminance Range	0.01 to 2,500,000 cd/m^2
Measurement Time	6 ms to 30 secs
Color Accuracy	±0.0015 in CIE 1931 x, y
Minimum Measuring Area	0.02 mm
Minimum Working Distance (w/Std. Lens)	356 mm

Chapter 3 Light Emissions from Flexible Polymer Composites Stimulated by Different Stresses

3.1 Introduction

Solid-state lighting based on LED has been increasingly utilized as energy saving sources in our daily life, such as general illumination and backlight for liquid-crystal display[115]. Currently, white light is typically obtained from phosphor-converted method that a GaN-based blue LED coupling with a yellow light phosphor layer (e.g., YAG: Ce)[116]. Generally, the white light source used in this technique is consisted of p-n junction based blue LED and LED pumped inorganic phosphor, which are both rigid in nature. Therefore, it is fascinating to explore new strategies with the configurations beyond the existing semiconductor p-n junction based structure. Particularly, it would be more attractive if the light sources with flexible feature can be triggered by multiple stimuli, such as uniaxial and biaxial mechanical

stresses. Such flexible optical devices are promising for many applications, including self-powered and energy harvesting optical systems, remote sensing without making electric contact, smart skin, bio-labels in response to pressure and flow.

According to the excitation sources, luminescence can be classified as PL, EL and ML, and so on. Compared to the PL and EL studies, ML has attracted much less attention so far. One of the reasons is that ML phosphors have suffered from destructive and poorly reproductive features. Fortunately, the introduction of EML materials which can emit light during elastic deformation without fracture allows us to have a further investigate the ML with various mechanical stimuli. Up to now, Xu's group has developed a series of EML phosphor materials with different emission colors which show the potential in a range of applications, such as stress sensor, optical imaging, artificial skin, and structural health diagnosis[58,62]. Among these ML materials, metal ion-doped ZnS phosphor has attracted much attention due to its sensitive response to mechanical stress with bright visible color emission[60,61,64]. Besides that, ZnS is also an excellent semiconductor which has been widely used in

the piezo-photonic devices. Recently, Wang coined a new research field of piezo-photonics in which a three-way coupling among piezoelectricity, luminescence and semiconductor behavior can tune the charge transport behavior and then improve the performance of optoelectronic devices[101,102,117,118]. In this chapter, various flexible composites of metal ion-doped ZnS phosphors mixed into PDMS matrix have been prepared which feature flexible, durable, easy and cost-effective fabrication with no use of vacuum, and compatible with arbitrary substrate. With these merits of the composite phosphors, we have further designed and fabricated light-emitting device from the composite phosphor-based hybrid structure free of p-n junction. White and green luminescence can be observed under multiple external stimuli including uniaxial strain of stretch and release, mechanical writing, and piezoelectric biaxial strain.

3.2 Sample fabrication and multiple mechanical stimuli

3.2.1 Fabrication of the flexible phosphor composite

The flexible phosphor composite was made of metal ion-doped ZnS particles and PDMS. Single-phase metal ion-doped ZnS powders (green: ZnS:Al,Cu (GGS42) or white: ZnS:Al,Cu,Mn (GG73), Global Tungsten & Powders Corp.) were homogenously mixed into a PDMS matrix. The PDMS consists of base and crosslink at a weight ratio of 10:1. Consequently, metal ion-doped ZnS based powders and the PDMS host comprise the flexible phosphor composite. The ratio of phosphor and PDMS was optimized at 7:3. Such an optimized value was obtained from numerous experiment results, which is a compromise between elastic module and luminescence.

3.2.2 Multiple mechanical stresses

Figure 3.1 shows a basic strategy for light-emissions from the flexible phosphor composite under different stimuli in this work. Various flexible composites contained metal ion (e.g., Cu, Al, and Mn) doped ZnS phosphor and PDMS matrix

are used here. It is known that ZnS is an excellent optoelectronic semiconductor. Furthermore, ZnS also exhibits piezoelectric effect due to its non-central symmetric wurtzite structure, resulting in piezoelectric potential when applying strain. PDMS chosen here works as a packaging material to encapsulate the metal ion-doped ZnS particles and transmit external stimuli to the luminescent centers. PDMS features high flexibility, high optical transparent, durable and low cost characteristics, which has widely been used in the fields of flexible solar cell, biological sensor and piezoelectric nanogenerators[119,120]. In our experiments, this metal ion-doped ZnS+PDMS flexible composite can be either used individually or coated on arbitrary substrates. Therefore, piezo-photonic luminescence device using PMN-PT wafer can be designed and fabricated. These structures will be simply triggered by various types of stimuli to generate light emission. Figure 3.1 shows four kinds of stimuli acting on the metal ion-doped ZnS+PDMS flexible composite, including electric field, uniaxial strains of stretch and mechanical writing, and piezoelectric biaxial strain. Light emissions can be recorded by a digital camera and various

spectrometers as shown in Figure 3.1. Consequently, the fabricated composite can be employed as a basic component for multiple purposes which will be described as follows.

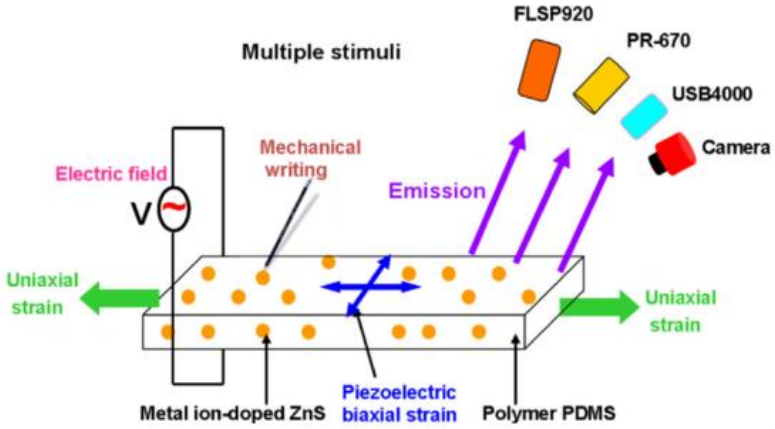

Figure 3.1 Schematic strategy of light-emissions from the flexible phosphor composite under different stimuli.

3.3 Uniaxial strain and mechanical writing induced luminescence

3.3.1 Fabrication of the flexible phosphor composite

The flexible phosphor composite was synthesized by mixing metal ion-doped

ZnS particles into PDMS matrix. Single-phase metal ion-doped ZnS powders (green: ZnS:Al,Cu (GGS42) or white: ZnS:Al,Cu,Mn (GG73), Global Tungsten & Powders Corp.) were homogenously mixed into a PDMS matrix. The PDMS consists of base and crosslink at a weight ratio of 10:1. Consequently, metal ion-doped ZnS based powders (70 wt. %) and the PDMS host (30 wt. %) comprise the flexible phosphor composite.

An Ocean Optics USB4000 CCD spectrometer was used to measure the luminescence spectra. A spectroradiometer (PR-670, Photo Research Inc.) was used to measure color properties, including Commission Internationale de L'Eclairage (CIE) coordinates, luminance and correlated colour temperature (CCT). The light-emitting images were captured by a digital camera (Sony Nex-5T). For the uniaxial strain measurement, a home-made stretching-releasing (S-R) system was used, which was composed of a stretch and release platform, as well as a step motor with variable stretching rate.

3.3.2 Results and discussion

Compared to extensively studied PL and EL, there has been limited report on the white light luminescence triggered by mechanical strain, because most of the ML phenomena are weak and irreproducible. Fortunately, the introduction of EML materials allows us to develop novel phosphors which are capable of converting mechanical stress into light emission. In this work, the flexible composite layer consisted of metal ion-doped ZnS and PDMS was stimulated by uniaxial strain of stretch and release, resulting in the white and green light emissions.

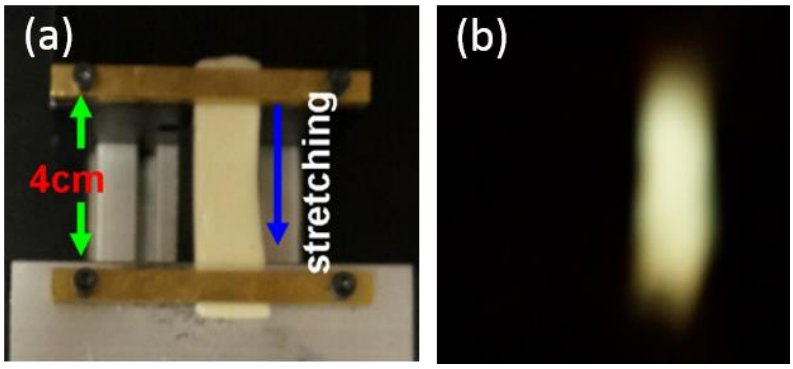

Figure 3.2 (a) Sample mounted on the S-R system, (b) white light-emission from the flexible phosphor composite under the stretch stress.

Figure 3.2a shows the flexible phosphor composite layer with an unstretched length of 4 cm mounted on the S-R system. When the step-motor is operated, the composite is first stretched to one direction and then returned. Such a complete process is regarded as one cycle here. Then the step-motor would repeat the motion in a pre-set period. Light emission can be observed, as Figure 3.2b shows. The blurred image is mainly due to the sample's motion.

Figure 3.3a shows white light emission spectra of the flexible phosphor composite at the S-R rate between 100 and 400 cycles per minute (cpm). Apparently, the white ML spectra consist of two main peaks at 525 nm and 588 nm, which are slightly different from the EL spectra composed of main peaks at 512 nm and 588 nm. Furthermore, a minor shoulder band located at around 460 nm in the EL spectrum is not apparent in the ML[121]. It is speculated that the frequency of S-R system is not high enough to activate the blue emission peaked at 460 nm sufficiently[64], as the rate of 400 cpm is approximately equivalent to 6.7 Hz, which is far less than the voltage frequency of 1 kHz on EL device.

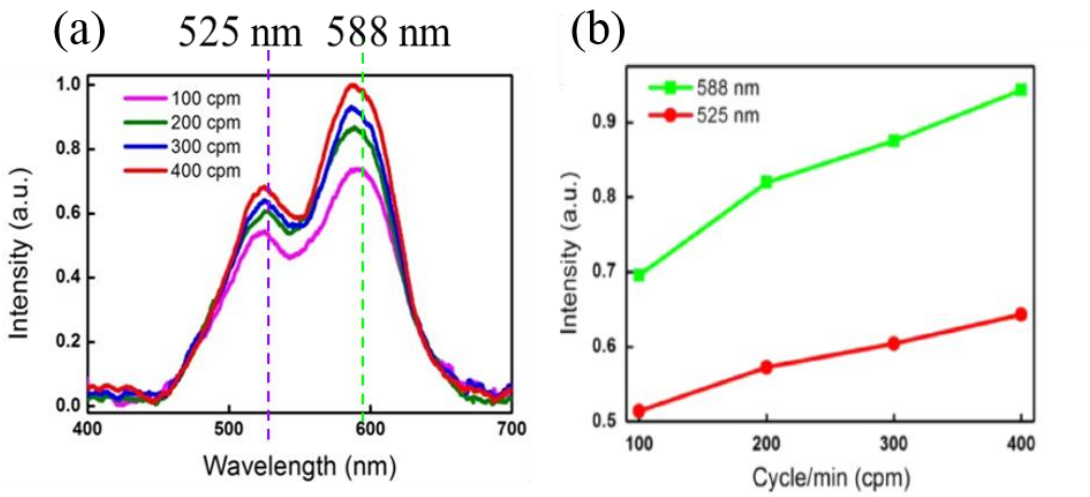

Figure 3.3 (a) Luminescence spectra of the sample at the S-R rate of 400 cpm. (b) Luminescence intensity peaked at 525 nm and 588 nm as a function of S-R rate.

Noticeably, ML intensities at both two peaks increase linearly with the increasing S-R rate. It is suggested that the emission intensity of luminescence is proportional to the strain and its rate of strain change induced by mechanical stress. More charge carriers are de-trapped with increasing S-R rate, resulting in the enhancement of electron-hole recombination[122]. It seems that luminescence intensities at two peak wavelengths are increased with different slope as the S-R rate ranges from 100 to 400 cpm (Figure 3.3b). The emission peak at 525 nm is due to

the D-A pairs recombination between $Al_{Zn} \rightarrow Cu_{Zn}$, while the radiation transition $^4T_1 \rightarrow {}^6A_1$ of Mn^{2+} ion dominates the emission peak at 588 nm. At the same S-R rate, the spontaneous transition probability of Cu and Mn ions may differ, leading to different enhancement factor in luminescence. Besides, another possible reason is associated with the green emission at 525 nm which might be more scattered by PDMS layer.

Table 3.1. Comparison of white light emissions between EL and ML.

Luminescence type	CIE (x, y)	CCT (K)	Luminance (cd/m^2)
EL	(0.3386, 0.3167)	5165	47
ML	(0.3397, 0.3466)	5196	21

It is helpful to understand the colour characteristics of the sample by measuring the CIE coordinates. The CIE and CCT of the composite under uniaxial strain were measured to be (0.3397, 0.3466) and 5196 K, respectively. The results indicate that the ML emitted from the flexible composite can be regarded as a cool white light. Jeong et al. have reported a wind-driven ML device that can emit warm, neutral, and

cool white colours by using the mixture of two blue and orange phosphors mixed to polymer[64]. They utilized the high velocity of wind energy belonging to the hurricane or typhoon to produce white light. Comparatively, in our experiment, only single-phase phosphor is mixed to PDMS, and white-light has been demonstrated in the composite phosphor harvesting the mechanical energy, which has the advantages of easy carrying out and low cost.

As the white light can be used for both backlight in display system and general lighting, it is fruitful to compare the colour properties of EL and ML from the flexible ZnS:Al,Cu,Mn+PDMS composite as shown in Table 3.1. Here the flexible EL device was operated at an external voltage of 100 V and 1 kHz, and the ML was measured at the S-R rate of 400 cpm. Different luminescence spectra of EL and ML should be responsible for the measured data listed in Table 1. According to the table, both CIE coordinates and CCT of ML are not exactly same as those of EL. The major cause of the difference is likely that the stretching stress during ML measurement is insufficient to activate the blue emission because of the softness of

PDMS as above mentioned. Compared to ML, EL device has different luminescence process and works at higher frequency, which benefits to the blue light emission. At any rate, both ML and EL of the synthesized composite phosphor could be considered as large-area white light sources, differing from commonly used white LED point source where a diffuser is usually needed in application.

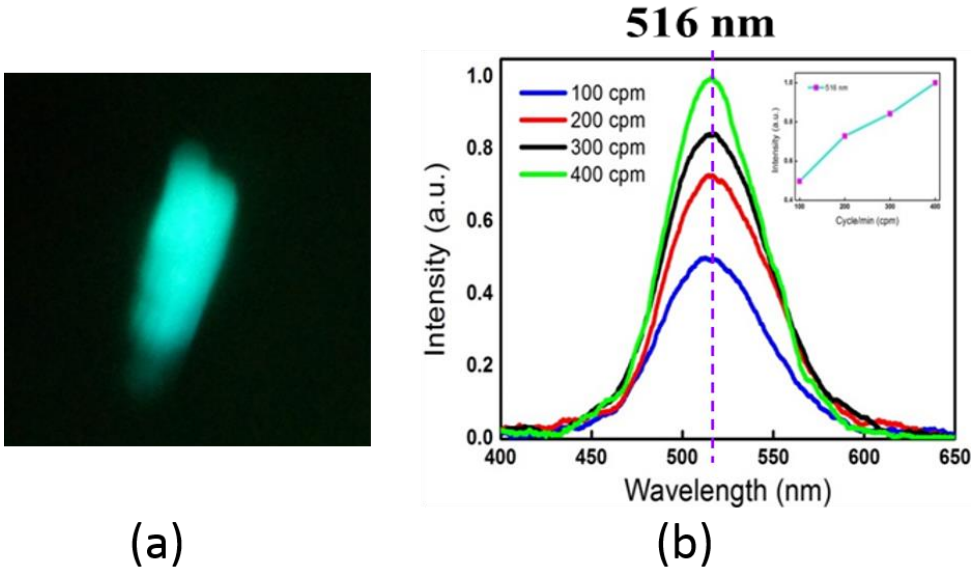

Figure 3.4 Luminescence spectra of the flexible phosphor composite. The inset shows the luminescence intensity peaked at 516 nm as a function of S-R rate.

Similarly, we mixed another green phosphor of Al and Cu ions co-doped ZnS

into PDMS. After well prepared, the green phosphor composite was mounted on the S-R system. Bright green light was seen by the naked eyes during the S-R process as shown in Figure3.4a. The green light peaked at 516 nm as shown in Figure 3.4b is due to the D-A recombination of $Al_{Zn} \rightarrow Cu_{Zn}$. The inset of Figure 3.4b shows the ML intensity of the composite as a function of S-R rate. It seems that the luminescence intensity is increased linearly with the S-R rate, which is consistent with the result as shown in Figure 3.3b.

Very recently, triboelectric effect has been explored to generate electricity through the conversion of ambient mechanical energy[123]. Therefore, it is interesting to investigate whether the mechanical friction can be used for generating light. Firstly, the above composite phosphor was spin-coated on a paper. Then the tip scribed across the paper gently (Fig. 3.5a), and finally a bright green light emitted from the contact area of the film was observed by the naked eyes (Fig. 3.5b).

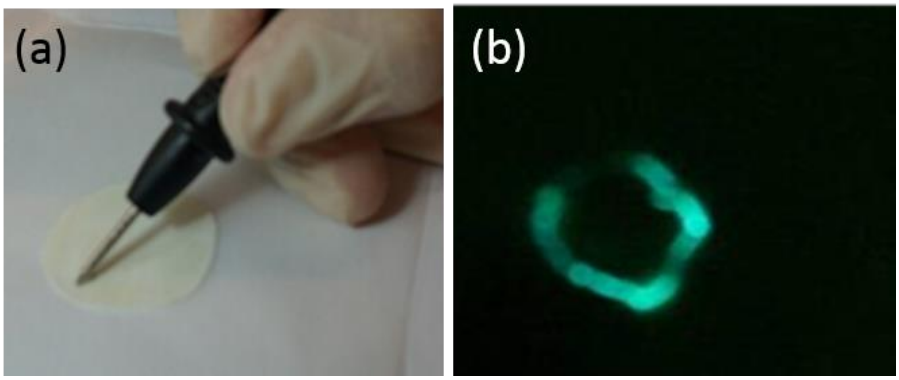

Figure 3.5 (a) Photograph of sample under mechanical writing, (b) Green light emission under mechanical writing.

3.4 Piezoelectric biaxial strain induced luminescence

3.4.1 Fabrication of light emission hybrid device

The PMN-PT substrate based piezo-photonic luminescence device was fabricated with a simply process. A PMN-PT single crystal oriented (001) (Hefei Kejing Material Technology Co., Ltd.) with the dimension of 5 mm×5 mm×0.5 mm was used as the substrate. Au electrodes with thickness of 100 nm and 200 nm were deposited by sputtering technique on the top and bottom surface of PMN-PT, respectively. The flexible phosphor composite was spin-coated on the PMN-PT

substrate and cured at 70 ℃ for 30 min.

The luminescence spectra of the hybrid device were measured by an Edinburgh FLSP920 spectrophotometer. A spectroradiometer (PR-670, Photo Research Inc.) was used to measure colour properties, including CIE coordinates, luminance and CCT. In the piezo-photonic luminescence device, the PMN-PT substrate which can provide biaxial strain to the phosphor composite was polarized with a Keithley 2410 high-voltage source meter. When applying an external voltage, the ac voltage was amplified by a high voltage linear power supplies (KEPCO Inc.). The light-emitting images were captured by a digital camera (Sony Nex-5T).

3.4.2 Results and discussion

It is well known that, PMN-PT is an excellent piezoelectric material. It features with large piezoelectric coefficient (d_{33} >2000 *p*C/N) and high electromechanical coupling factor (k_{33} >0.9). Hence, PMN-PT single crystal is capable of producing a large strain under an external bias voltage. Our previous studies indicate that it is

feasible to deliver the strain provided by PMN-PT to a variety of functional thin films and 2D materials[103,124,125]. It should be pointed out that the strain provided by the piezoelectric effect is biaxial, which is homogeneous in *x* and *y* directions of the sample[126-128]. Such a piezoelectric strain is different from the above mentioned uniaxial strain produced by stretching or friction. Biaxial strain has previously been reported to induce remarkable changes in band structure and therefore greatly enhance luminescence compared to uniaxial one[129-131]. Herein, it should be helpful to compare the luminescence behaviors of the composite phosphor under different types of strains, namely uniaxial and biaxial strains. Furthermore, we may design and fabricate on-wafer piezoelectric luminescence device by taking the advantage of the PMN-PT piezoelectric actuator. With this mind, a piezoelectric luminescence device composed of the above flexible composite phosphor has been demonstrated in this part.

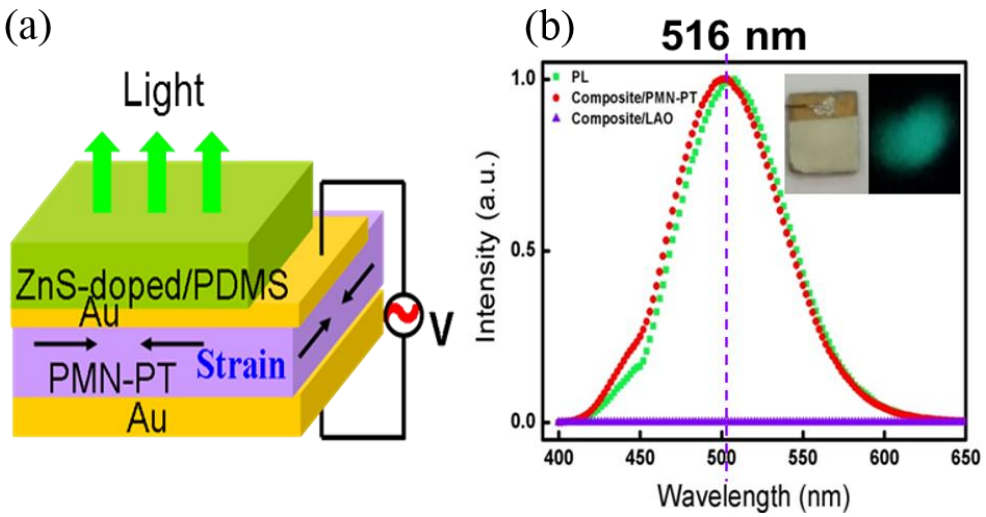

Figure 3.6 (a) Device structure of Au/PMN-PT/Au/ZnS+PDMS. (b) Luminescence spectra of PL and ML from the sample. The inset shows the tested sample and light-emission under an applied voltage of 400 V_{pp} and 400 Hz.

As shown in the Figure 3.6a, the PMN-PT single-crystal was sandwiched between two gold electrodes. Subsequently a layer of doped-ZnS+PDMS composite was spin-coated on the top electrode. In order to positively polarizing the PMN-PT single crystal, a dc voltage (500 V) was applied to the substrate in advance. Owing to the converse piezoelectric effect of PMN-PT substrate, the lattice deformation

caused by electric field can impose in-plane strain to the doped-ZnS+PDMS composite. As semiconductor ZnS with a wurtzite structure exhibits a non-central symmetric structure, the substrate-imposed strain can induce a piezoelectric potential and subsequently stimulate luminescence[103].

Figure 3.6b illustrates the luminescence spectrum of the ZnS:Al,Cu+PDMS composite when an AC voltage of 400 V_{pp} at 400 Hz was applied on PMN-PT. Photographs of the actual tested sample of the hybrid structure device and light emission are also included in the insets. During the retention of the ac voltage, the strain applied on the above hybrid structure is changed periodically. As a consequence, ZnS:Al,Cu+PDMS triggered by the biaxial strain arising from PMN-PT emits light, as shown in Figure 3.6b. For comparison, a non-piezoelectric insulator $LaAlO_3$ (LAO) was employed to substitute PMN–PT in this system. As expected, no obvious luminescence was observed, further supporting the operation principle of biaxial strain-induced luminescence. The PL spectrum of ZnS:Al,Cu composite phosphor used in this hybrid device is also shown for comparison. The

two similar spectra suggest the same dominant emission peaked at 516 nm, which is stemmed from the D-A recombination of $Al_{Zn} \rightarrow Cu_{Zn}$[132,133].

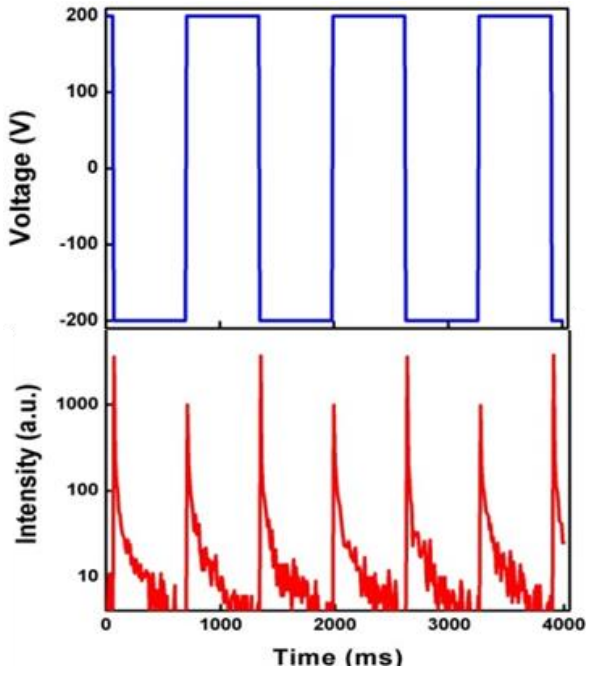

Figure 3.7 Luminescence intensity peaked at 508 nm as a function of time when a square-wave voltage is applied.

Figure 3.7 presents the transient luminescence of the hybrid structure device when applying a square voltage on PMN-PT. Pulsed emissions can be observed in the device stimulated by a square voltage. The peak intensity of luminescence

appears when the bias is switched on or off, indicating the strain-induced luminescence is essentially a dynamic process when a time-varying voltage is applied. Moreover, luminescence intensity peaks are corresponded to both the rising and falling edges of the square voltage. This observation differs from our previous studies on the PLD grown oriented ZnS: Mn^{2+} thin film structure which has intensity peak only at the falling edges of the square voltage[103]. The mechanism may be related to the polycrystalline ZnS powder with random orientation in this experiment. After reaching a maximum value, the emission intensity decreases exponentially with time. Such a change in the luminescence intensity can be expressed as[134]:

$$I = I_0 \exp[-\chi_t (t - t_0)] \qquad (3.1)$$

Where I_0 is the luminescence intensity at $t = t_0$, $\chi = 1/\tau$, and τ is the lifetime of carrier.

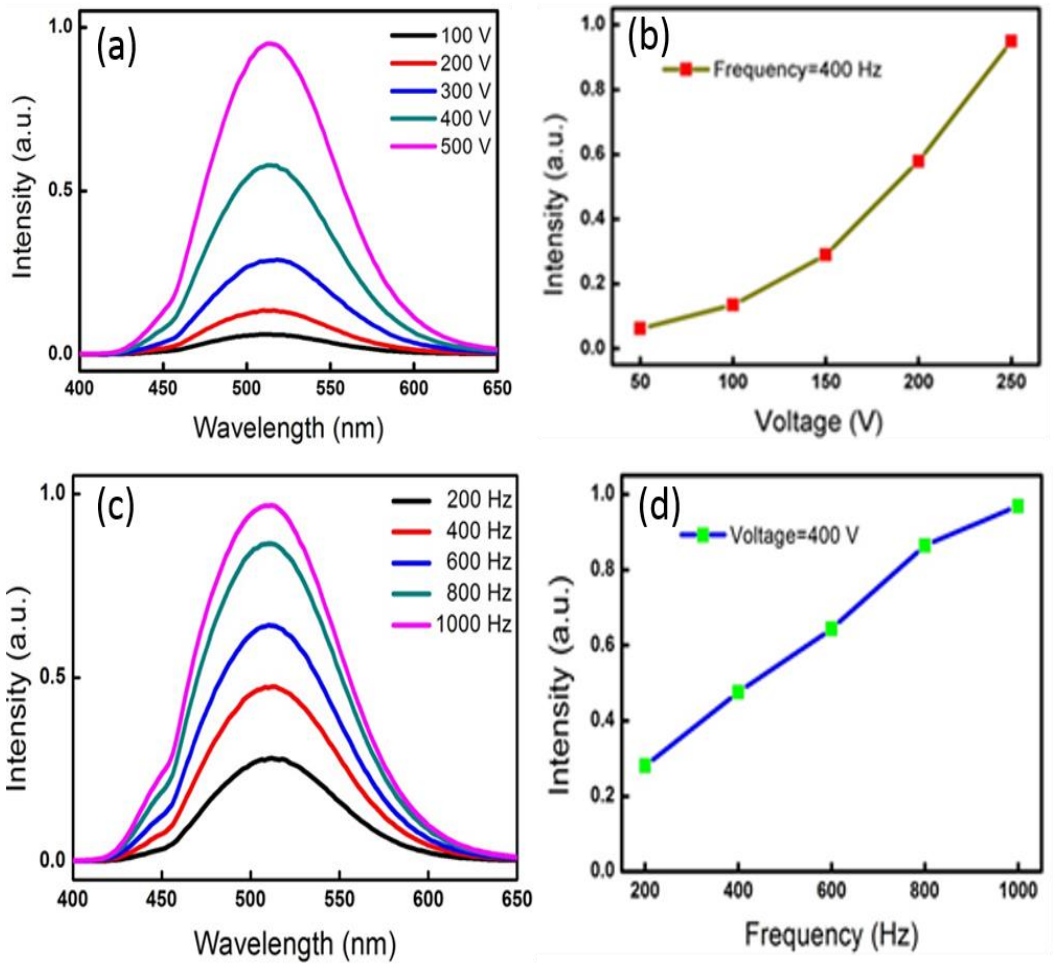

Figure 3.8 (a) Luminescence spectra of sample under different voltages at 400 Hz. (b) Luminescence intensity peaked at 508 nm responses as a function of voltage at 400 Hz. (c) Luminescence spectra of sample under different frequency at 400 V_{pp}. (d) Luminescence intensity peaked at 508 nm responses as a function of frequency at 400 V_{pp}.

Figure 3.8a shows the luminescence spectra of the device triggered under the bias voltage varying from 100 to 500 V. Note that the luminescence intensity of ZnS:Al,Cu+PDMS composite enhances when increasing the applied voltage as shown in Figure 3.8b. Similar trend was also found for the measuring frequency dependence of luminescence intensity when the frequency is increased from 200 to 1000 Hz (Figure 3.8c and d). In the measurements, the increase in luminescence intensity did not show any sign of saturation with the increase in voltage and frequency within the measurement range. This observation is similar to the study on the light emissions of ZnS:Mn and ZnS:Cu phosphors under pressure, which is caused from self-recovery of the de-trapped charges[122]. Compared to the luminescence from the flexible phosphor composite under uniaxial strain, the light-emission from PMN-PT based piezo-photonic emission device here can be precisely controlled, which can also work at high frequency.

Similarly, we replaced the phosphor composite with Cu, Mn, and Al co-doped ZnS into PDMS matrix, which was used as the phosphor layer and spin-coated on

the top gold electrode.

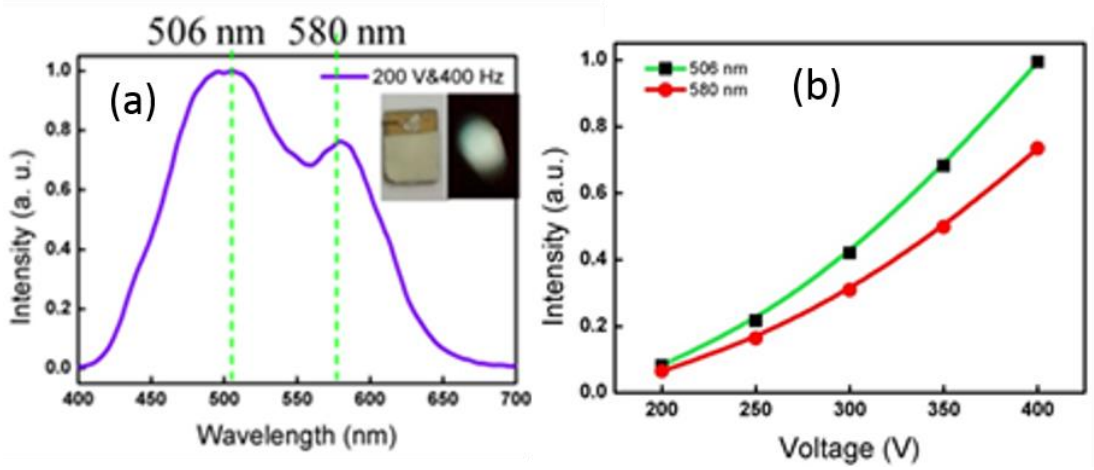

Figure 3.9 (a)White light emission spectrum from the hybrid device of Au/PMN-PT/Au/ZnS+PDMS under the electric field. (b) Luminescence intensities peaked at 506 nm and 580 nm response as a function of voltage at 400 Hz.

After applied a square voltage of 200 V and the frequency of 400 Hz, white light emits from the surface of the phosphor layer, Figure 3.9a illustrates the luminescence spectrum of the with light, and insets were the photographs of the piezoelectric device and the white light emission. The spectrum in Figure 3.9a shows two main peaks of 506 nm and 580 nm. As above discussed for the energy transition

mechanism of the EL sample, the emission peak at 506 nm is due to the D-A pairs recombination between $Al_{Zn} \rightarrow Cu_{Zn}$, while the radiation transition $^4T_1 \rightarrow {}^6A_1$ of Mn^{2+} ion dominates the emission peak at 580 nm. Light intensity increased lineally with increasing external voltage as Figure 3.9b shows.

3.5 Conclusions

In conclusion, a kind of flexible phosphor composites have been synthesized by mixing metal ion-doped ZnS phosphor into transparent PDMS matrix. Under uniaxial stretch stress, white light emission with CIE coordinates (0.3397, 0.3466) and CCT of 5196 K is obviously seen by the naked eyes in the flexible composite composed of single-phase ZnS:Al,Cu,Mn. When increasing S-R rate, the intensities of main emission peaks are enhanced, and therefore the overall white light becomes brighter. Interestingly, the developed composite phosphor can sense or harvest broad mechanical energy, including stretch, vibration pressure and mechanical friction. The observed luminescence of piezo-photonic luminescence device is originated from

piezoelectric potential induced by PMN-PT substrate, and the luminescence intensity is strongly dependent on not only the rate of biaxial strain change, but also the magnitude and frequency of the voltage applying upon the PMN-PT wafer. The works suggest our developed flexible composite phosphors and devices have the potential for the applications in the fields of novel white light source, energy harvesting, anti-counterfeiting and self-powered illumination system.

Chapter 4 Tuning PL of AIE Material via Mechanical Stresses

4.1 Introduction

Tuning luminescence of phosphor materials has attracted widespread interest in various research fields, including optical sensing, information storage, solid-state illumination and display, as well as bioimaging. In these applications, it is highly desirable to change one or more of the emission characters, such as wavelength, intensity and lifetime. So far, conventional chemical approaches have routinely been employed to manipulate the luminescence during the phosphor's synthesis by changing chemical compositions, nanocrystal size, crystal structure and phase, and so on. Despite the chemical approach is an effective way to modify the luminescence, it suffers from the limitation of ex-situ and irreversible processes or the difficulty in understanding the kinetic processes of how the luminescence changes with band energy, crystal structural symmetry, and crystal field. In contrast to chemical

approach, however, physical methods providing precise control over the process of modification luminescence properties by applying mechanical stress, magnetic field, electric field, temperature, ionizing radiation, and so on[13].

The AIE phenomenon is opposite to the aggregation-caused quenching, which makes it advanced applications in optoelectronics, biomedical probes, and chemical sensors. An appealing feature of many AIEgens are smart materials, which change their luminescence properties in response to external stimuli, such as mechanical force, photonic irradiation, electric field, solvent polarity, temperature, pH and fuming[35,135,136]. The luminescence change of AIEgens with mechanical force is known as mechanochromic luminogens. TPE and its derivatives are well-studied mechanochromic luminogens. Previous work has focused only on the phenomenon of grinding leads to a color shift in the emission of AIE powder and thermal annealing or vapor fuming by a polar solvent reverses the emission color[137], only a few studies report the pressure caused color change in a small range[77,83,138]. Here we expand the way of mechanical stresses to tuning light emission of TPE derivative

thin film by utilizing biaxial strain and uniaxial stress provided PMN-PT piezoelectric single crystal and magnetic polymer composite, respectively. Our approach based on the dynamic control of stress transfer via reverse piezoelectric effect and magnetostrictive effect, which offers precise ways to tuning color emission of the TPE derivative thin films in real-time and in-situ.

4.2 Tuning PL through piezoelectric strain

4.2.1 Device fabrication based on the PMN-PT substrate

N,N-diphenyl-4-(1,2,2-triphenylvinyl)aniline (DPA-TPE) was offered by Benzhong Tang's group. The DPA-TPE crystals were dissolved in the trichloromethane ($CHCl_3$) solvent by magnetic stirring for 30 min. A PMN-PT single crystal oriented (001) (Hefei Kejing Material Technology Co., Ltd.) with the dimension of 5 mm 5 mm 0.5 mm was used as the substrate. Gold thin films were deposited on the surface of PMN-PT as top and bottom electrodes. Then a layer of

AIE thin film was spin-coated on the PMN-PT substrate and annealed in oven at 140℃ for 20 min.

Characterization: the structure of the compound was characterized by ^{1}H and ^{13}C NMR, mass spectrometry, and elemental analysis. The PL emission spectrum was measured by an Edinburgh FLSP920 spectrophotometer.

4.2.2 Results and discussion

TPE is one of the well-studied AIEgens, which has a common configuration as HPS. As Figure 4.1a shows, four phenyl rings are linked to a central ethene rod through rotatable C-C single bonds and can rotate or twist against the ethane stator freely[19]. Theoretical calculations and experiments have verified that the RIR process leads to the AIE effect of TPE. In other words, when the intramolecular rotations of the aromatic rings are hindered, the emission of the AIEgen is enhanced[36,77,139].

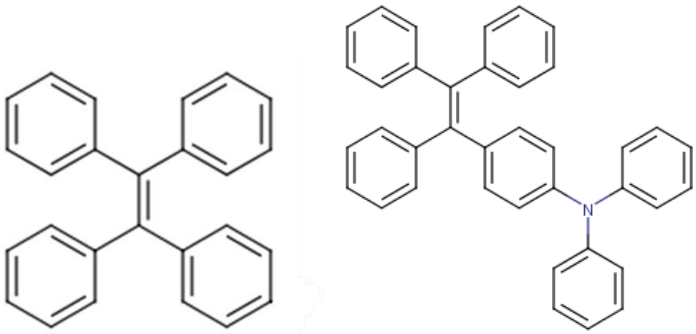

(a) (b)

Figure 4.1 Diagram of molecular structures of (a) TPE and (b) DPA-TPE.

DPA-TPE is a kind of derivative which has similar molecular structure (Figure 4.1b) as TPE. To confirm whether a compound has AIE effect or not, the PL spectrum is typically studied by the method of adding a poor solvent into the solution of the compound[138]. DPA-TPE compound has a good solubility in $CHCl_3$, while being insoluble in water. The emission spectrum of a dilute solution of DPA-TPE in $CHCl_3$ is shown in Figure 4.2, which peaks at 470 nm. When a large amount of water is added into the solution, intense emission is observed. It is notably that a significant enhancement of luminescence is observed in the water/$CHCl_3$ mixture with water fraction >60%. As DPA-TPE is insoluble in water, increasing the water

fraction can cause the aggregated of the molecules in the mixtures. With the water content above 50%, the DPA-TPE molecules may cluster together to form ordered, crystalline aggregates while they start form random, amorphous aggregates after the water content exceeds 70% as the inset shows in Figure 4.2. Apparently, the PL emission of DPA-TPE compound is enhanced by aggregate formation, which shows that it is AIE-active.

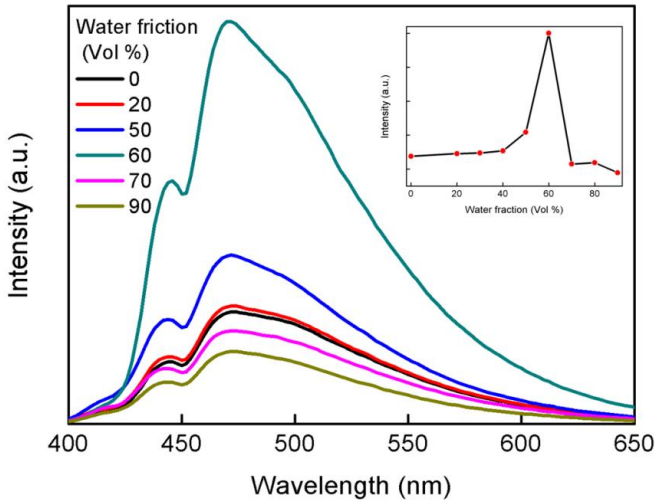

Figure 4.2 PL spectra of DPA-TPE with different water friction at room temperature under 365 nm UV light irradiation. Inset is the plot of PL intensity versus the water proportion from 0 to 90%.

The mechanochromic effect of some AIEgens observed in the grinding experiment[138] inspires us to explore the fluorescence property of DPA-TPE compound with piezoelectric strain. As aforementioned, the PMN-PT single crystal exhibits excellent ferroelectric polarization and converse piezoelectric, as well as outstanding electromechanical coupling factors[140]. Here, the thin film of DPA-TPE with a thickness of 200 nm was spin-coated on the PMN-PT substrate as shown in Figure 4.3. For comparison, a silicon wafer substrate which has no piezoelectricity has been used to replace the PMN-PT with similar device structure: Au/Si/SiO_2/Au/DPA-TPE/PMMA.

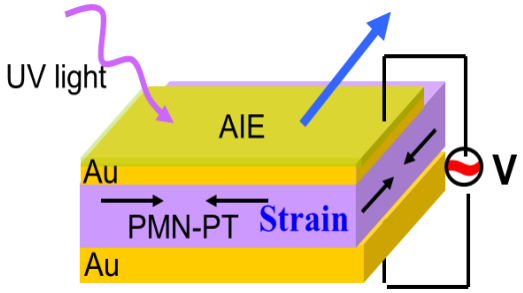

Figure 4.3 Device structure of Au/PMN-PT/Au/DPA-TPE/PMMA.

In order to obtain a good piezoelectricity, PMN-PT was prior polarization by

applying a dc voltage of 500 V. The polarized ferroelectric PMN-PT single crystals exhibit excellent converse piezoelectric effect with a piezoelectric coefficient of d_{33} >2000 pC/N. This means that when an electric field with the same (opposite) polarity as the poling field to the ferroelectric materials, and expansion (compression) lattice strain along the direction of the electric field will be induced due to the converse piezoelectric effect[141]. Notably, a positive electric field can produce an in-plane compressive strain in the PMN-PT substrate. The magnitude of the lattice strain in the PMN-PT substrate can be calculated by the equation of by combining Bragg's law and Poisson ratio from the XRD results under electric field[142]. Theoretical and experimental results have suggested that the substrate-induced lattice strain has a linear dependence on the bias voltage with a slope of 0.04% per 100 V[125,143].

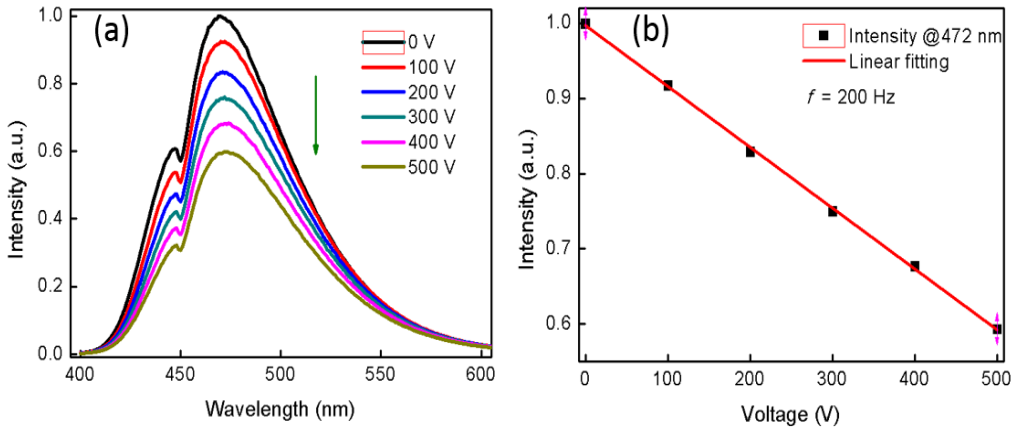

Figure 4.4 (a) PL emission spectra from the Au/PMN-PT/Au/DPA-TPE/PMMA device with various voltages from 0 to 500 V. (b) PL emission peak as a function of voltage from the Au/PMN-PT/Au/DPA-TPE/PMMA device.

When a sinusoidal electric field was applied to the polarized PMN-PT substrate, due to the converse piezoelectric effect of PMN-PT substrate, the externally applied electric field can cause a lattice deformation which induced in-plane strain. The induced strain can be effectively delivered to the up layer of DPA-TPE thin film and caused a compressive strain in the thin film, resulting in a decrease in the PL emission intensity of DPA-TPE. PL spectrum of the DPA-TPE thin film was

measured under externally applied electric field. Figure 4.4a shows the PL emission spectra from the PMN-PT based hybrid device with various voltages from 0 to 500 V, under the illumination of 365 nm UV light. The PL spectral shape and peak position are practically unaffected by the piezoelectric strain derived from PMN-PT substrate, indicating that the basic molecular structure of DPA-TPE is unaltered. The PL intensity of DPA-TPE thin film, however, is sensitive to the applied piezoelectric strain. Notably, the PL intensity decreases linearly with increasing voltage as Figure 4.4b shows. Under a voltage of 500 V, the PL intensity decreased by 40%. For comparison, a non-piezoelectric material silicon oxide was employed to substitute PMN–PT in this system. As expected, no obvious PL spectrum change was observed, implying that the intensity decrease not results from electric field but the piezoelectric strain from PMN-PT.

The influence of frequency of the electric field on the PL emission of DPA-TPE thin film has also been investigated. As Figure 4.5 demonstrates, the PL intensity decreases swiftly with increasing frequency of electric field, which has a similar

variation tendency as voltage. When the frequency reaches to 3000 Hz, the intensity has decreased by 42% (Figure 4.6). After that frequency, the emission has little change. No emission peak shifts during the piezoelectric strain applying process. The PL intensity will recover by annealing or fuming.

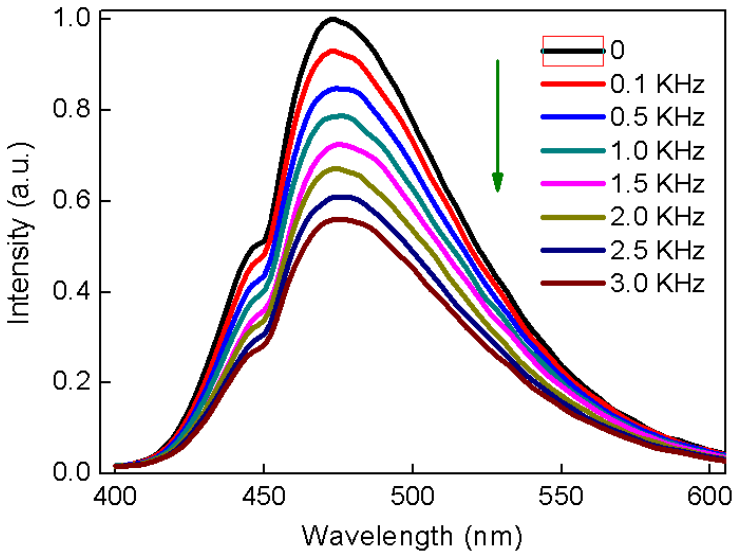

Figure 4.5 PL emission spectra from the Au/PMN-PT/Au/DPA-TPE/PMMA device with various frequencies of electric field from 100 Hz to 3000 Hz.

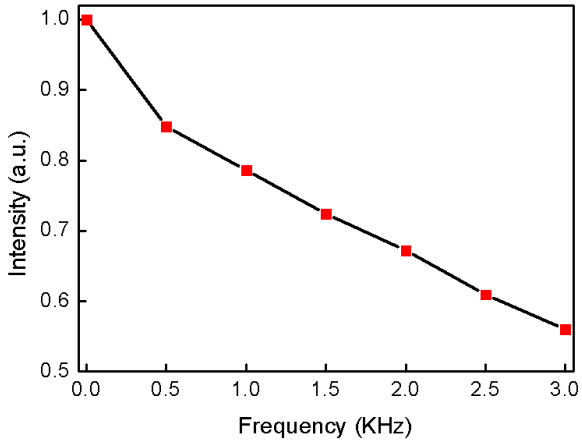

Figure 4.6 PL emission peak as a function of frequency of electric field from the Au/PMN-PT/Au/DPA-TPE/PMMA device with the voltage of 200 V.

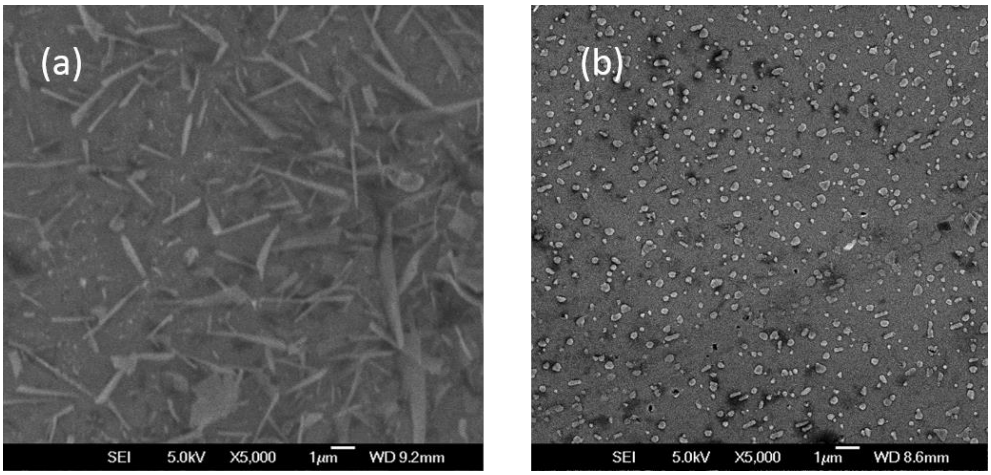

Figure 4.7 SEM images of DPA-TPE thin film on the PMN-PT substrate before (a) and after (b) applied an external electric field on the substrate.

The microstructure structure of the DPA-TPE thin film is shown in the SEM image of Figure 4.7. It is noted that, after applied an external electric field on the PMN-PT substrate, the morphology of the DPA-TPE has significant change from crystalline to amorphous, leading to a weaken of PL emission intensity. When an external electric field applied the piezoelectric single crystal of PMN-PT substrate, a piezoelectric strain induced by the in-plane biaxial strain from PMN-PT substrate will deliver to the DPA-TPE thin film. It is deduced that the piezoelectric strain activates the vibration motions of AIE molecular, resulting in luminescence quenching[77].

4.3 PL modification via magnetostrictive stress

In addition to the above electric-induce piezoelectric effect techniques, the application of magnetism is another common method to tune the emission from DPA-TPE phosphors. An early work reported by Singh et al. on magnetic tuning the PL intensity of Gd_2O_3:Yb/Er nanoparticles, which decreased eight-fold under a dc

magnetic field with strength of 1 T[144]. Recently, Yunxin Liu et al. has reported the magnetic tuning effect based on $NaGdF_4$:Nd/Yb/Er nanoparticles, whose emission intensity was decreased to 60% and 15% at 300 K and 10 K under a 12 KOe magnetic field, respectively[17]. In their work, large magnetic field has been utilized, as well as low temperature. Recently, our group has realized the magnetism induced luminescence from polymer phosphor composite via magnetostrictive strain at low magnetic field and room temperature. Here, the magnetism and stress has been coupled to tuning luminescence in the form of magnetostrictive strain from the Fe-Co-Ni compound. This work opens a new path to investigate the relationship between magnetism and AIE molecular. The results show a promising application of AIE phosphor materials in the magnetic sensor and detectors.

4.3.1 Device fabrication based on the magnetic composite

DPA-TPE was offered by Benzhong Tang's group. The DPA-TPE crystals were dissolved in the $CHCl_3$ solvent by magnetic stirring for 30 min. Then the solution

was spin-coated on a glass sheet with the rotate speed of 1000 rpm and annealed in oven at 140℃ for 20 min. On the other hand, the Fe-Co-Ni alloy particles with the average size of 100 μm were embedded into uncured PDMS matrix with a weight ratio of 2.5:1. Then the magnetic polymer composite was spin-coated on the surface of DPA-TPE thin film and annealed at 70℃ for 2 h.

Characterization: A Lakeshore 7400 VSM was used to measure the magnetic properties of the magnetic polymer composite magnetic field ranging from -15 to 15 kOe at room temperature. Stress induced from the magnetic polymer composite was measurement by a stress sensor (Wogu digital force gauge Zu-50). A digimatic indicator (Mitutoyo 112 AMB) was employed to characterize the strain induced from the magnetic composite. The PL spectra were recorded using an Ocean optics spectrometer USB4000 charged coupled device (CCD) spectrophotometer (JEOL, Japan) spectrophotometer. All the measurements were proceeded at room temperature.

4.3.2 Results and discussion

The Mechanochromic effect of some AIEgens[138] prompts us to explore the fluorescence property of DPA-TPE compound with various kinds of stress. Here, we have taken advantage of the magnetostrictive stress from magnetic polymer composite consisted of Fe-Co-Ni alloy nanoparticles and PDMS to tuning the PL emission of DPA-TPE thin film in magnetic field.

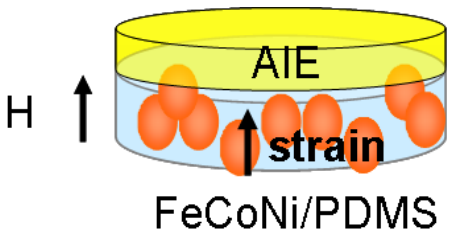

Figure 4.8 Structure of DPA-TPE/Fe-Co-Ni+PDMS composite.

As Figure 4.8 shows, a layer of DPA-TPE thin film with a thickness of 50 nm was spin-coated on the surface of the magnetic polymer composite. The magnetic composite made of Fe-Co-Ni alloy nanoparticles and PDMS matrix can generate large deformation under the stimulus of external magnetic. PDMS used here serves

as a packaging material. In the meantime, it can deliver the generated strain from magnetic part to the DPA-TPE phosphor part under magnetic field. When an external magnetic field is applied on the composite, the magnetorstrictive strain will be generated along the direction of magnetic field. The magnetic-induced stress can deliver to the DPA-TPE thin film worked as a compressive stress. In order to well understand the magnetic actuator property of the magnetic polymer composite, the magnetic and elastic properties have been measured under static magnetic field.

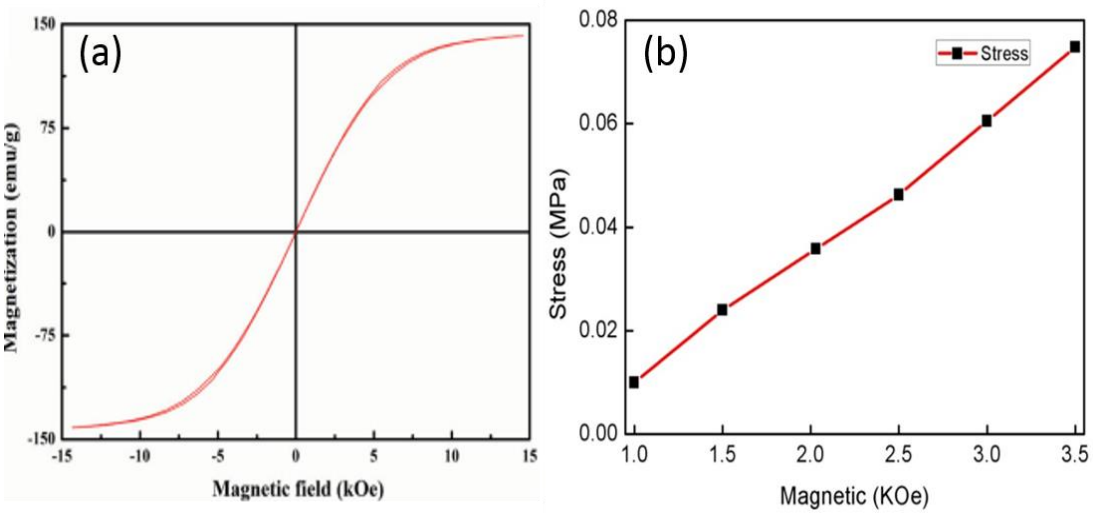

Figure 4.9 (a) Magnetization of the Fe-Co-Ni+PDMS magnetic polymer composite. (b) Stress from the Fe-Co-Ni+PDMS magnetic polymer composite as a function of

applied magnetic field.

The chosen Fe-Co-Ni alloys are typically soft magnetic materials which exhibit a very low coercive field and high saturation magnetization. The magnetization curve of Fe-Co-Ni+PDMS magnetic polymer composite is demonstrated in Figure 4.9a, measured by VSM at room temperature. When the magnetic polymer composite is applied a magnetic field within the range of several kOe, it shows a nearly linear magnetic behavior with no significant hysteresis for a negligible coercive field of 9 Oe. This is a desirable feature in generating stress in our experiment since the residual magnetization could be avoided[63]. Figure 4.9b shows the elastic properties of Fe-Co-Ni +PDMS composite with the magnetic field varies from 1 to 3.5 KOe. It indicates that the stress increased monotonous with increasing magnetic field strength. As our home-made magnetic actuator's maximum output magnetic field strength is 3.5 KOe, which corresponds to a stress of 0.08 MPa from the magnetic.

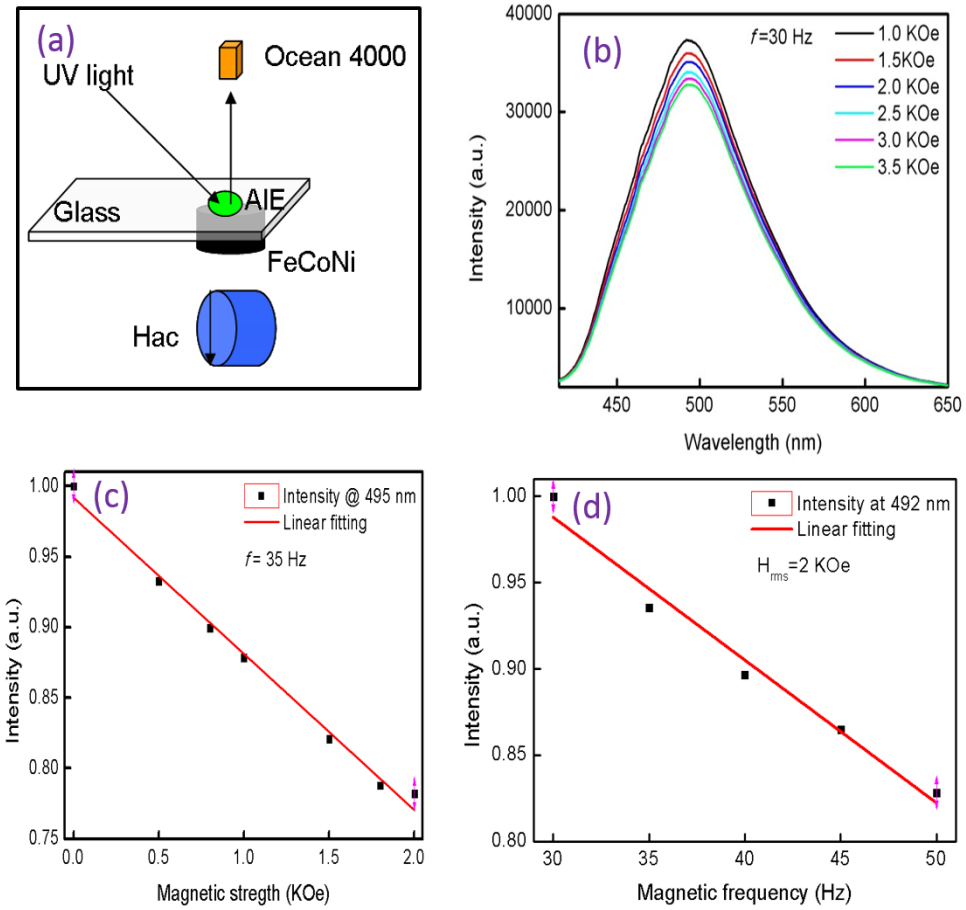

Figure 4.10 (a) Scheme of the setup used to tune the PL emission of DPA-TPE under magnetic field. (b) PL spectra from DPA-TPE thin film under magnetic field. (c) PL intensity of DPA-TPE thin film as a function of magnetic field strength. (d) PL intensity of DPA-TPE thin film depends on the modulation frequency of magnetic field.

A time-varying magnetic field was provided by rotating an NdFeB permanent magnet with a controller. The 365 nm UV light was delivered to the surface of DPA-TPE thin film using an optical fiber, while the PL emissions were collected by another optical fiber (shown in Figure 4.10a). Figure 4.10b presents that the green light from DPA-TPE thin film can be efficiently tuned by the applied magnetic field at room temperature. The intensity of PL emission has a linearly decreasing as the magnetic field strength in the range of 0 to 2 KOe. It is noted that, when the applied magnetic field reached up 2 KOe, the luminescent intensity could decrease to ≈78% (shown in Figure 4.10c). When the magnetic field strength is fixed at 2 KOe, the PL emission intensity has a similar decreasing trend with varying magnetic frequency as Figure 4.10d shows. At the magnetic frequency of 50 Hz, the PL intensity decreased 17%, compared its original emission intensity without magnetic field.

Magnetostrictive stress tuning the PL emission is mainly due to the compression of DPA-TPE thin film. The compression stress can reduce the distances of adjacent molecules and increase molecular interactions, leading to the enhance of

electronic orbital overlapping, spin-orbital coupling and spin flipping, which will populate the triplet state and activate energy transfer, resulting in luminescence quenching[77].

4.4 Conclusion

In this chapter, we have investigated two different ways to tuning PL emission intensity of DPA-TPE thin film in the form of piezoelectric strain and magnetostrictive stress by electric field and magnetic field, respectively. Both the two methods can efficiently tune the PL emission intensity at room temperature, with PL emission intensity decreased to 60% and 78% of its original intensity at 500 voltage electric field and 2 KOe magnetic field strength, respectively. A phase transition from crystalline to amorphous state has been observed during applying of mechanical stresses. The results indicate the DPA-TPE compounds have promising applications in electric and magnetic sensing and detections.

Chapter 5 PL Modification of Organic-Inorganic Halide Perovskite

5.1 Introduction

Halide perovskite semiconductors of the form AMX_3 (A =CH_3NH_3, Cs, etc.; M = Pb, Sn; X = Cl, Br, I) have recently emerged as a promising class of materials for solar cell applications. In particular, since their first appearance in 2009 as light-absorbing materials for sensitized solar cells, $CH_3NH_3PbX_3$ based perovskites have attracted attention because of their rapid increase in photoconversion efficiency[145]. Through its development, perovskite materials have come to feature high absorption coefficients, long carrier lifetimes and diffusion lengths, ambipolar carrier transport, and shallow defect levels. With these exceptional attributes, it becomes a competitive optoelectronic material for applications in photovoltaics, light emitting diodes (LED), photodetectors, lasers, and more[42]. Despite the rapid increase in $MAPbX_3$ solar cell efficiency associated with more and more applications in

optoelectronic devices, optimization and full characterization of devices continues to be a major assignment for researchers. In general, the photophysical processes in these materials are still far from being understood. It is known that light[110,146], oxygen and humidity have effect on the performance of solar cell device and thin film structure. However, the effect of strain on the perovskite thin film has been little reported. As it is reported giant stress can make phase transition and emission peak shift in perovskite single crystal[96,147,148]. In this work, we investigated the piezoelectric strain-induced PL enhancement in $CH_3NH_3PbI_3$ ($MAPbI_3$) thin film.

5.2 PL modification from $CH_3NH_3PbI_3$ thin film

5.2.1 Fabrication of Au/PMN-PT/Au/$MAPbI_3$/PMMA device

Two layers of Au electrodes were deposited on the bottom and top sides of PMN-PT substrate by magnetron sputtering. The PMN-PT substrate was then polarized by a dc voltage of 500 V for 15 min. After that, the top surface of the PMN-PT was treated by O_2 plasma for 5 min. The $MAPbI_3$ film was formed by spin

coating a mixed precursor solution of methylammonium iodide (MAI) and lead chlorine ($PbCl_2$) with a molar ratio of 3:1 (0.88 M lead chloride) in N, Ndimethylformamide (DMF), followed by thermal annealing at 100ºC for 45 min in the glovebox. The $MAPbI_3$ film was covered by a layer of PMMA and dried at 70 ºC for 30 min.

Keithley 2400 High Voltage Supply was used for the poling process of PMN-PT substrate and applied electric field on the device during testing. The PL spectrum was tested by an Edinburgh FLSP920 spectrophotometer. 485 nm laser was used as excitation light source during the PL measurement.

5.2.2 Results and discussion

As aforementioned, PMN-PT single crystal has superior piezoelectric property. Here, we utilize the piezoelectric strain induced by PMN-PT substrate to tuning the PL emission of organic-inorganic halide perovskite $MAPbI_3$ thin film. The designed hybrid device structure combining $MAPbI_3$ thin film and PMN-PT single crystal is

shown in Figure 5.1.

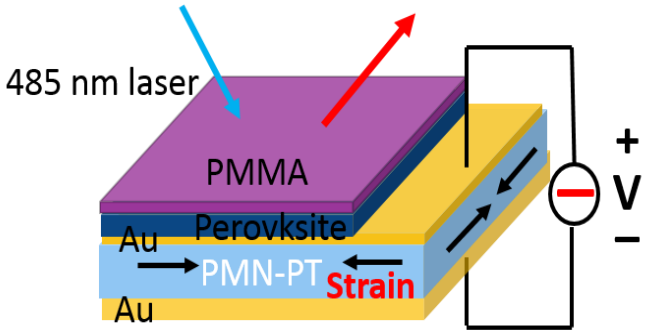

Figure 5.1 Device structure of Au/PMN-PT/Au/$MAPbI_3$ /PMMA.

The thicknesses of up gold electrode and $MAPbI_3$ thin film are 50 nm and 300 nm, respectively. The piezoelectric strain offered by the PMN-PT substrate can be effectively delivered to the up layer of perovskite thin film. The PMMA layer used here is to prevent the perovskite thin film from the oxygen and humility. The PMN-PT substrate has been previously polarized by a 500 V dc voltage so that the dominant in the crystal has been ordered orientation. During the experiment process, when applied an external dc electric field on the PMN-PT substrate, a biaxial strain is induced and delivers to the $MAPbI_3$ thin film, resulting in PL intensity enhancement.

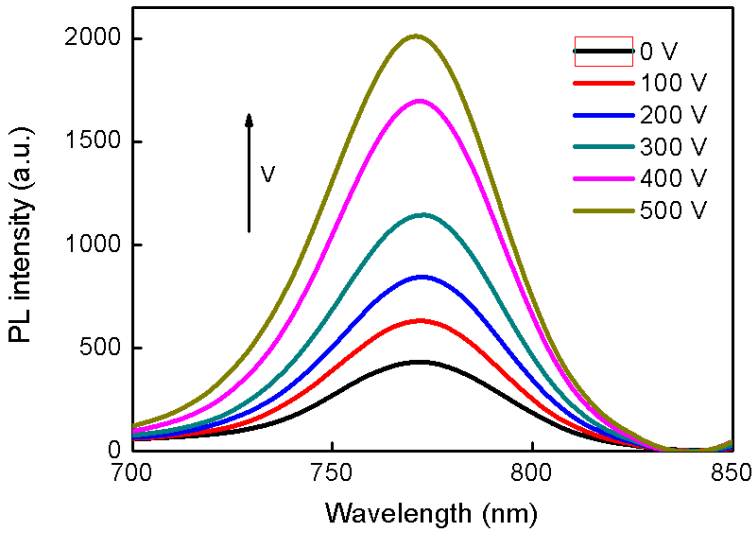

Figure 5.2 PL emission spectra of $MAPbI_3$ thin film under different electric voltage, 485 nm laser was used as the excitation light source.

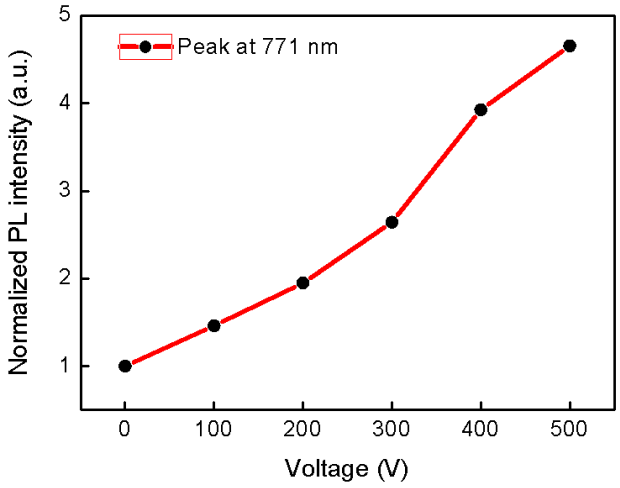

Figure 5.3 PL intensity peaked at 771 nm from the $MAPbI_3$ thin film dependence on the applied electric voltage.

At ambient conditions, the sample was irradiated by a 5 mW laser at 485 nm. A red emission peaked at 771 nm can be detected, which is consistent with previous literature[51]. When a dc electric field was applied on the PMN-PT substrate, the PL emission intensity increased with increasing voltage as Figure 5.2 shows. Figure 5.3 shows the emission intensity peaked at 771nm increases monotonously when the voltage varies from 0 to 500 V. Note that the PL intensity peak is almost 5 times larger at the voltage of 500 V than the original PL emission intensity without external electric field. Above 500 V, the PL intensity almost unchanged. After tuning off the electric field, the PL intensity kept at a center value which is larger than the original PL emission intensity.

As the structure of $MAPbX_3$ perovskite consists of a MX_6 octahedral and organic ammonium cations in the A site, the organic ammonium is unstable under external excitation and may introduce some defects during the crystallization process. The reason for the biaxial strain induced the brightening of $MAPbI_3$ thin film may be related to ion migration[110,111], or the decreasing of surface defects[149,150] which

generated in the synthesize process of thin film.

5.3 Conclusion

In this chapter, we studied the light response of the organic-inorganic halide perovskite, $MAPbI_3$, as a function of biaxial piezoelectric strain supplied by PMN-PT single crystal substrate. 5 times enhancement from the PL spectrum intensity has been observed under the electric voltage of 500 V, which could be attributed to the tilting of PbI_6 octahedral and the destroying of long-range ordering of MA cations. The results show that the biaxial piezoelectric strain has positive affect on the light emission of perovskite thin film. This demonstration not only provides a new insight and fundamental understanding on the light property of organic-inorganic halide perovskites, but also sheds light on the development of brightness optoelectronic devices.

Chapter 6 Conclusions and Suggestions for Future Work

6.1 Conclusion

The present research focused on the investigation of optical properties and modulation of smart materials. The main conclusions can be briefly summarized as follows:

A kind of flexible composite phosphors has been synthesized by mixing metal ion-doped ZnS phosphor into transparent PDMS matrix. Under uniaxial stretch stress, white light emission with CIE coordinates of (0.3397, 0.3466) and CCT of 5196 K is obviously seen by the naked eyes in the flexible composite composed of single-phase ZnS: Al,Cu,Mn. When increasing S-R rate, the intensities of main emission peaks are enhanced, and therefore the overall white light becomes brighter. Interestingly, the developed composite phosphor can sense or harvest broad mechanical energy, including stretch, vibration pressure, and mechanical friction. Therefore, a kind of

light-emission device, piezo-phototronic luminescence device (metal ion doped ZnS+PDMS composite/Au/PMN-PT/Au) has been designed and fabricated. The observed luminescence of piezo-photonic luminescence device is originated from piezoelectric potential induced by PMN-PT substrate, and the luminescence intensity is strongly dependent on not only the rate of biaxial strain change, but also the magnitude and frequency of the voltage applying upon the PMN-PT wafer. The works suggest our developed flexible composite phosphors and devices have the potential for the applications in the fields of novel white light source, energy harvesting, anti-counterfeiting, and self-powered illumination system.

Piezoelectric strain and magentostrictive stain were used to tuning PL emission intensity of DPA-TPE thin film. The DPA-TPE thin film was spin-coated on the PMN-PT substrate which could induce piezoelectric strain under the external electric field. The PL intensity was linearly decreasing with the external electric field and only remained 60% of its original emission intensity at 500 V of the electric field. The PL intensity decrease arises from the piezoelectric strain delivers from the

PMN-PT substrate to the DPA-TPE thin film. In addition, the magnetic field can modulate the PL intensity of DPA-TPE thin film when it integrated with magnetic polymer composite in room temperature. The PL intensity decreased to 78% of its original value at a low magnetic field strength of 2 KOe. These results indicate the DPA-TPE compounds have promising applications in electric and magnetic sensing and detections.

A strain-induced PL enhancement in methylammonium lead iodide ($CH_3NH_3PbI_3$) thin film spin-coated on the PMN-PT substrate has been investigated. The PL intensity peaked at 771 nm is 5 times of the original one without piezoelectric biaxial strain. The reason may be that the biaxial strain has reduced the defects of the perovskite surface. This work provides an in-situ and dynamic way to control PL under electric field.

6.2 Suggestions for future work

This thesis focuses on studying optical properties and tuning spectral properties of the smart phosphors. There is plenty room needing further research. The following are some suggestions for further research which may be regarded as an extension of the present work.

The ability to excite the flexible polymer composite consisted of metal ion-doped ZnS phosphor and PDMS matrix through PMN-PT substrate is of great interest for photoelectron devices application. As the white light emission from the polymer phosphor composite is due to the piezoelectric strain induced by the PMN-PT substrate. By optimizing the structure of polymer phosphor composite and PMN-PT substrate, it is promising to harvest the white light by applying low voltages to PMN-PT substrate at its resonance working mode.

A new approach has been utilized to modulation the PL emission of AIE piezoelectric phosphor materials by combing with piezoelectric single crystal PMN-PT or magnetostrictive polymer composite. This result leads us to consider other

form of strain to tune the luminescence of AIE. For example, spin-coat the AIE thin film on flexible PET substrate, subsequently blend the sample with stretch or compression strain. In future work, it is necessary to investigate other form of mechanical strain like stretch and compression to tuning the PL emission of AIE materials.

We have demonstrated the mechanical strain to modulate the PL emission of one kind of AIE materials, DPA-TPE thin film. As the AIE materials contain a lot of stress sensitive derivatives and most of them present reversibility color change in response to mechanical grinding. Therefore, in future work, the investigation on the piezoelectric strain induced modulation of other AIE materials will be conducted.

The piezoelectric strain generated from PMN-PT single crystal has been utilized to tuning the PL emission of organic-inorganic perovskite, resulting in the enhancement of light intensity. As light emission devices such as halide perovskite based LEDs have been widely studied in recent years, it is significant to use

appropriate mechanical stresses to modulation or enhance the luminous efficiency of EL from the halide perovskites materials in the future.

References

1 Harry K. Wright, G. V. E. *Photoluminescence research progress*. (Nova Science Publishers, Inc., 2008).

2 Reichman, J. *Handbook of Optical Filters for Fluorescence Microscopy* (Chroma Technology, 2010).

3 Lakshmanan, A. *Luminescence and Display Phosphors*. (Nova Science Publishers, Inc., 2008).

4 Yen, Shionoya, S., Yamamoto, H. & Yen, W. M. *Phosphor Handbook*. (2007).

5 Vecht, A., Werring, N. & Smith, P. High-efficiency dc electroluminescence in ZnS (Mn, Cu). *Journal of Physics D: Applied Physics* **1**, 134 (1968).

6 Virk, H. S. History of Luminescence from Ancient to Modern Times. *Defect and Diffusion Forum* **361**, 1-13 (2015).

7 Chandra, B. P. in *Luminescence of Solids* (ed D. R. Vij) 361-389 (Springer US, 1998).

8 Zhang, H., Yamada, H., Terasaki, N. & Xu, C.-N. Green mechanoluminescence of $Ca_2MgSi_2O_7$:Eu and $Ca_2MgSi_2O_7$:Eu,Dy. *Journal of The Electrochemical Society* **155**, J55-J57 (2008).

9 Xu C. N., W. T., Akiyama M., Zheng X. G. Artificial skin to sense mechanical stress by visible light emission. *Applied Physics Letters* **74**, 1236-

1238 (1999).

10 C.N. Xu, T. W., M. Akiyama, X.G. Zheng. Preparation and characteristics of highly triboluminescent ZnS film. *Material Research Bulletin* **34**, 1491-1500 (1999).

11 Xu, C.-N., Zheng, X.-G., Akiyama, M., Nonaka, K. & Watanabe, T. Dynamic visualization of stress distribution by mechanoluminescence image. *Applied Physics Letters* **76**, 179-181 (2000).

12 Zhang, J. C., Xu, C. N. & Long, Y. Z. Elastico-mechanoluminescence in $CaZr(PO_4)_2:Eu^{2+}$ with multiple trap levels. *Opt Express* **21**, 13699-13709 (2013).

13 Bai, G., Tsang, M.-K. & Hao, J. Tuning the luminescence of phosphors: beyond conventional chemical method. *Advanced Optical Materials* **3**, 431-462 (2015).

14 Trotta, R. *et al.* Nanomembrane quantum-light-emitting diodes integrated onto piezoelectric actuators. *Adv Mater* **24**, 2668-2672 (2012).

15 Autler, S. H. & Townes, C. H. Stark effect in rapidly varying fields. *Physical Review* **100**, 703 (1955).

16 Takeuchi, T. *et al.* Quantum-confined Stark effect due to piezoelectric fields in GaInN strained quantum wells. *Japanese Journal of Applied Physics* **36**, L382 (1997).

17 Liu, Y., Wang, D., Shi, J., Peng, Q. & Li, Y. Magnetic tuning of upconversion luminescence in lanthanide-doped bifunctional nanocrystals. *Angew Chem Int Ed Engl* **52**, 4366-4369 (2013).

18 Tikhomirov, V. K. *et al.* Er^{3+}-doped nanoparticles for optical detection of magnetic field. *Nano letters* **9**, 721-724 (2009).

19 Mei, J. *et al.* Aggregation-induced emission: the whole is more brilliant than the parts. *Advanced Materials* **26**, 5429-5479 (2014).

20 Ngo, I.-L. & Byon, C. A review on enhancing thermal conductivity of transparent and flexible polymer composites. *Science of Advanced Materials* **8**, 257-266 (2016).

21 Zhang, Z. *et al.* Mesoporous piezoelectric polymer composite films with tunable mechanical modulus for harvesting energy from liquid pressure fluctuation. *Advanced Functional Materials* **26**, 6760-6765 (2016).

22 Noh, J.-S. Conductive elastomers for stretchable electronics, sensors and energy harvesters. *Polymers* **8**, 123 (2016).

23 Nan, C.-W., Bichurin, M. I., Dong, S., Viehland, D. & Srinivasan, G. Multiferroic magnetoelectric composites: historical perspective, status, and future directions. *J. Appl. Phys.* **103**, 031101 (2008).

24 Choi, M. Y. *et al.* Mechanically powered transparent flexible charge‐generating nanodevices with piezoelectric ZnO nanorods. *Advanced Materials* **21**, 2185-2189 (2009).

25 Curie, J. & Curie, P. Development by pressure of polar electricity in hemihedral crystals with inclined faces. *Bull. soc. min. de France* **3**, 90 (1880).

26 Zhang, R., Jiang, B. & Cao, W. Elastic, piezoelectric, and dielectric properties of multidomain $0.67Pb(Mg_{1/3}Nb_{2/3})O_3–0.33PbTiO_3$ single crystals.

J. Appl. Phys. **90**, 3471 (2001).

27 Jianhua Yin, B. J., Wenwu Cao. Elastic, piezoelectric, and dielectric properties of 0.955 $Pb(Zn_{1/3}Nb_{2/3})O_3$-0.45$PbTiO_3$ single crystal with designed multidomains. *IEEE* **47**, 285-291 (2000).

28 Park, S. E. & Shrout, T. R. Relaxor based ferroelectric single crystals for electro-mechanical actuators. *Materials Research Innovations* **1**, 20-25 (1997).

29 Luo, H., Xu, G., Xu, H., Wang, P. & Yin, Z. Compositional homogeneity and electrical properties of lead magnesium niobate titanate. *Japanese Journal of Applied Physics* **39**, 5581-5585 (2000).

30 Hong, Y., Lama, J. W. Y. & Tang, B. Z. Aggregation-induced emission. *Chemical Society Reviews* **40**, 5361–5388 (2011).

31 Hu, R., Leung, N. L. C. & Tang, B. AIE macromolecules: syntheses, structures and functionalities. *Chem Soc Rev* **43**, 4494-4562 (2014).

32 O'Neill, M. & Kelly, S. M. Liquid crystals for charge transport, luminescence, and photonics. *Advanced Materials* **15**, 1135-1146 (2003).

33 Yuan, W. Z. *et al.* High efficiency luminescent liquid crystal: aggregation-induced emission strategy and biaxially oriented mesomorphic structure. *Journal of Materials Chemistry* **22**, 3323-3326 (2012).

34 Ding, D., Li, K., Liu, B. & Tang, B. Z. Bioprobes based on AIE fluorogens. *Accounts of chemical research* **46**, 2441-2453 (2013).

35 Wang, M., Zhang, G., Zhang, D., Zhu, D. & Tang, B. Z. Fluorescent

bio/chemosensors based on silole and tetraphenylethene luminogens with aggregation-induced emission feature. *Journal of Materials Chemistry* **20**, 1858-1867 (2010).

36 Chen, J. *et al.* Synthesis, light emission, nanoaggregation, and restricted intramolecular rotation of 1, 1-substituted 2, 3, 4, 5-tetraphenylsiloles. *Chemistry of materials* **15**, 1535-1546 (2003).

37 Li, Z. & Qin, A. Diverge from the norm. *National Science Review* **1**, 22-24 (2014).

38 Luo, J., Song, K., long Gu, F. & Miao, Q. Switching of non-helical overcrowded tetrabenzoheptafulvalene derivatives. *Chemical Science* **2**, 2029-2034 (2011).

39 Im, J.-H., Lee, C.-R., Lee, J.-W., Park, S.-W. & Park, N.-G. 6.5% efficient perovskite quantum-dot-sensitized solar cell. *Nanoscale* **3**, 4088-4093 (2011).

40 Kim, H.-S. *et al.* Lead iodide perovskite sensitized all-solid-state submicron thin film mesoscopic solar cell with efficiency exceeding 9%. *Scientific reports* **2**, 591 (2012).

41 Yang, W. S. *et al.* High-performance photovoltaic perovskite layers fabricated through intramolecular exchange. *Science* **348**, 1234-1237 (2015).

42 Chen, Q. *et al.* Under the spotlight: the organic–inorganic hybrid halide perovskite for optoelectronic applications. *Nano Today* **10**, 355-396 (2015).

43 Veldhuis, S. A. *et al.* Perovskite materials for Light-Emitting Diodes and lasers. *Adv Mater* **28**, 6804-6834 (2016).

44 Frost, J. M. *et al.* Atomistic origins of high-performance in hybrid halide perovskite solar cells. *Nano letters* **14**, 2584-2590 (2014).

45 Brivio, F., Walker, A. B. & Walsh, A. Structural and electronic properties of hybrid perovskites for high-efficiency thin-film photovoltaics from first-principles. *APL Materials* **1**, 042111 (2013).

46 Leijtens, T. *et al.* Electronic properties of meso-superstructured and planar organometal halide perovskite films: charge trapping, photodoping, and carrier mobility. *ACS nano* **8**, 7147-7155 (2014).

47 Stranks, S. D. *et al.* Electron-hole diffusion lengths exceeding 1 micrometer in an organometal trihalide perovskite absorber. *Science* **342**, 341-344 (2013).

48 Dong, Q. *et al.* Electron-hole diffusion lengths >175 μm in solution-grown $CH_3NH_3PbI_3$ single crystals. *Science* **347**, 967-970 (2015).

49 Stranks, S. D. *et al.* Recombination kinetics in organic-inorganic perovskites: excitons, free charge, and subgap states. *Physical Review Applied* **2**, 034007 (2014).

50 Kitazawa, N., Watanabe, Y. & Nakamura, Y. Optical properties of $CH_3NH_3PbX_3$ (X=halogen) and their mixed-halide crystals. *Journal of materials science* **37**, 3585-3587 (2002).

51 Tan, Z.-K. *et al.* Bright light-emitting diodes based on organometal halide perovskite. *Nature nanotechnology* **9**, 687-692 (2014).

52 Yantara, N. *et al.* Inorganic halide perovskites for efficient light-emitting diodes. *J. Phys. Chem. Lett* **6**, 4360-4364 (2015).

53 Protesescu, L. *et al.* Nanocrystals of cesium lead halide perovskites ($CsPbX_3$, X= Cl, Br, and I): novel optoelectronic materials showing bright emission with wide color gamut. *Nano letters* **15**, 3692-3696 (2015).

54 Hassan, Y. *et al.* Structure-tuned lead halide perovskite nanocrystals. *Advanced Materials* **28**, 566-573 (2016).

55 Peng, D., Chen, B. & Wang, F. Recent advances in doped mechanoluminescent phosphors. *ChemPlusChem* **80** (2015).

56 Sohn, K.-S., Park, D. H. & Kim, J. S. Luminescence of pulsed-laser-deposited $SrAl_2O_4$:Eu,Dy thin film and its role as a stress indicator. *Journal of The Electrochemical Society* **152**, H161-H167 (2005).

57 Xu, C.-N., Watanabe, T., Akiyama, M. & Zheng, X.-G. Direct view of stress distribution in solid by mechanoluminescence. *Applied Physics Letters* **74**, 2414-2416 (1999).

58 Zhang, H., Yamada, H., Terasaki, N. & Xu, C.-N. Ultraviolet mechanoluminescence from $SrAl_2O_4$:Ce and $SrAl_2O_4$:Ce,Ho. *Applied Physics Letters* **91**, 081905 (2007).

59 Terasawa, Y., Xu, C. N., Yamada, H. & Kubo, M. Near Infra-Red mechanoluminescence from strontium auminate doped with rare-earth ions. *IOP Conference Series: Materials Science and Engineering* **18**, 212013 (2011).

60 Jeong, S. M., Song, S., Lee, S. K. & Ha, N. Y. Color manipulation of mechanoluminescence from stress-activated composite films. *Adv Mater* **25**, 6194-6200 (2013).

61 Moon Jeong, S., Song, S., Lee, S.-K. & Choi, B. Mechanically driven light-generator with high durability. *Applied Physics Letters* **102**, 051110 (2013).

62 Terasaki, N., Yamada, H. & Xu, C.-N. Ultrasonic wave induced mechanoluminescence and its application for photocatalysis as ubiquitous light source. *Catalysis Today* **201**, 203-208 (2013).

63 Wong, M. C., Chen, L., Tsang, M. K., Zhang, Y. & Hao, J. Magnetic-induced luminescence from flexible composite laminates by coupling magnetic field to piezophotonic effect. *Adv Mater*, 4488-4495 (2015).

64 Jeong, S. M. *et al.* Bright, wind-driven white mechanoluminescence from zinc sulphide microparticles embedded in a polydimethylsiloxane elastomer. *Energy Environ. Sci.* **7**, 3338-3346 (2014).

65 Wang, X. *et al.* Dynamic pressure mapping of personalized handwriting by a flexible sensor matrix based on the mechanoluminescence process. *Adv Mater* **27**, 2324-2331 (2015).

66 Terasaki, N., Zhang, H., Yamada, H. & Xu, C. N. Mechanoluminescent light source for a fluorescent probe molecule. *Chem Commun* **47**, 8034-8036 (2011).

67 Ma, Z., Wang, Z., Teng, M., Xu, Z. & Jia, X. Mechanically induced multicolor change of luminescent materials. *Chemphyschem* **16**, 1811-1828 (2015).

68 Zhang, X., Chi, Z., Zhang, Y., Liu, S. & Xu, J. Recent advances in mechanochromic luminescent metal complexes. *J. Mater. Chem. C* **1**, 3376 (2013).

69 Chi, Z. *et al.* Recent advances in organic mechanofluorochromic materials. *Chem Soc Rev* **41**, 3878-3896 (2012).

70 Todres, Z. V. Recent advances in the study of mechanochromic transitions of organic compounds. *J. Chem. Res.* **February**, 89-93 (2004).

71 Jiarui, X. & Zhenguo, C. *Mechanochromic fluorescent materials: phenomena, materials and applications*. (Royal Society of Chemistry, 2014).

72 Sagara Y., K. T. Mechanically induced luminescence changes in molecular assemblies. *Nat Chem* **1**, 605-610 (2009).

73 Li, C. *et al.* Reversible luminescence switching of an organic solid: controllable on-off persistent room temperature phosphorescence and stimulated multiple fluorescence conversion. *Advanced Optical Materials* **3**, 1184-1190 (2015).

74 Sun, H. *et al.* Smart responsive phosphorescent materials for data recording and security protection. *Nat Commun* **5**, 3601 (2014).

75 Yoon, S.-J. *et al.* Multistimuli two-color luminescence switching via different slip-stacking of highly fluorescent molecular sheets. *Journal of the American Chemical Society* **132**, 10747-10749 (2010).

76 Dong, Y. *et al.* Aggregation-induced and crystallization-enhanced emissions of 1,2-diphenyl-3,4-bis(diphenylmethylene)-1-cyclobutene. *Chem Commun* 3255-3257 (2007).

77 Fan, X. *et al.* Photoluminescence and electroluminescence of hexaphenylsilole are enhanced by pressurization in the solid state. *Chem Commun* 2989-2991 (2008).

78 Luo, X. *et al.* Reversible switching of the emission of diphenyldibenzofulvenes by thermal and mechanical stimuli. *Adv Mater* **23**, 3261-3265 (2011).

79 Han, T. *et al.* Defect-sensitive crystals based on diaminomaleonitrile-functionalized Schiff base with aggregation-enhanced emission. *J. Mater. Chem. C* **1**, 7314-7320 (2013).

80 Teng, M. J., Jia, X. R., Yang, S., Chen, X. F. & Wei, Y. Reversible tuning luminescent color and emission intensity: a dipeptide-based light-emitting material. *Adv Mater* **24**, 1255-1261 (2012).

81 Zhao, N. *et al.* A tetraphenylethene-substituted pyridinium salt with multiple functionalities: synthesis, stimuli-responsive emission, optical waveguide and specific mitochondrion imaging. *J. Mater. Chem. C* **1**, 4640-4646 (2013).

82 Zhao, N. *et al.* Benzothiazolium-functionalized tetraphenylethene: an AIE luminogen with tunable solid-state emission. *Chemical Communications* **48**, 8637-8639 (2012).

83 Dong, Y. Q., Lam, J. W. & Tang, B. Z. Mechanochromic luminescence of aggregation-induced emission luminogens. *The journal of physical chemistry letters* **6**, 3429-3436 (2015).

84 Michael M. Lee, J. T., Tsutomu Miyasaka, Takurou N. Murakami, Henry J. Snaith. Efficient hybrid solar cells based on meso-superstructured organometal halide perovskites. *Science* **338**, 643-647 (2012).

85 Burschka, J. *et al.* Sequential deposition as a route to high-performance perovskite-sensitized solar cells. *Nature* **499**, 316-319 (2013).

86 Woon Seok Yang, J. H. N., Nam Joong Jeon, Young Chan Kim,Seungchan Ryu, Jangwon Seo, Sang Il Seok. High-performance photovoltaic perovskite layers fabricated through intramolecular exchange. *Science* **348**, 1234-1237 (2015).

87 Deschler, F. *et al.* High photoluminescence efficiency and optically pumped lasing in solution-processed mixed halide perovskite semiconductors. *J Phys Chem Lett* **5**, 1421-1426 (2014).

88 Sadhanala, A. *et al.* Blue-green color tunable solution processable organolead chloride-bromide mixed halide perovskites for optoelectronic applications. *Nano Lett* **15**, 6095-6101 (2015).

89 Xing, G. *et al.* Low-temperature solution-processed wavelength-tunable perovskites for lasing. *Nat Mater* **13**, 476-480 (2014).

90 Sutherland, B. R. & Sargent, E. H. Perovskite photonic sources. *Nature Photonics* **10**, 295-302 (2016).

91 Noh, J. H., Im, S. H., Heo, J. H., Mandal, T. N. & Seok, S. I. Chemical management for colorful, efficient, and stable inorganic-organic hybrid nanostructured solar cells. *Nano Lett* **13**, 1764-1769 (2013).

92 Ogomi, Y. *et al.* $CH_3NH_3SnxPb_{(1-x)}I_3$ perovskite solar cells covering up to 1060 nm. *J Phys Chem Lett* **5**, 1004-1011 (2014).

93 Jeon, N. J. *et al.* Compositional engineering of perovskite materials for high-performance solar cells. *Nature* **517**, 476-480 (2015).

94 Hao, F., Stoumpos, C. C., Cao, D. H., Chang, R. P. H. & Kanatzidis, M. G. Lead-free solid-state organic–inorganic halide perovskite solar cells. *Nature*

Photonics **8**, 489-494 (2014).

95 Wang, Y. *et al.* Pressure-induced phase transformation, reversible amorphization, and anomalous visible light response in organolead bromide perovskite. *J Am Chem Soc* **137**, 11144-11149 (2015).

96 Capitani, F. *et al.* High-pressure behavior of methylammonium lead iodide ($MAPbI_3$) hybrid perovskite. *J. Appl. Phys.* **119**, 185901 (2016).

97 Li, H., Castelli, I. E., Thygesen, K. S. & Jacobsen, K. W. Strain sensitivity of band gaps of Sn-containing semiconductors. *Physical Review B* **91**, 045204 (2015).

98 Kuykendall, T. R., Schwartzberg, A. M. & Aloni, S. Gallium nitride nanowires and heterostructures: toward color-tunable and white-light sources. *Adv Mater* **27**, 5805-5812 (2015).

99 E. Fred Schubert, J. K. K. Solid-State Light Sources Getting Smart. *Science* (2005).

100 Zhang, J. C. *et al.* An intense elastico-mechanoluminescence material CaZnOS:Mn^{2+} for sensing and imaging multiple mechanical stresses. *Opt Express* **21**, 12976-12986 (2013).

101 Wang, Z. L. Piezopotential gated nanowire devices: piezotronics and piezo-phototronics. *Nano Today* **5**, 540-552 (2010).

102 Pan, C. *et al.* High-resolution electroluminescent imaging of pressure distribution using a piezoelectric nanowire LED array. *Nature Photonics* **7**, 752-758 (2013).

103 Zhang, Y. *et al.* Piezo-phototronic effect-induced dual-mode light and ultrasound emissions from ZnS:Mn/PMN-PT thin-film structures. *Adv Mater* **24**, 1729-1735 (2012).

104 Hideki Matsubara, S. Y., Hirohisa Saito, Yue Jianglin, & Yoshinori Tanaka, S. N. GaN photonic-crystal surface-emitting laser at blue-violet wavelengths. *Science* **319**, 445-447 (2008).

105 Deng, R. *et al.* Temporal full-colour tuning through non-steady-state upconversion. *Nat Nanotechnol* **10**, 237-242 (2015).

106 Hao, J., Zhang, Y. & Wei, X. Electric-induced enhancement and modulation of upconversion photoluminescence in epitaxial $BaTiO_3$:Yb/Er thin films. *Angewandte Chemie* **123**, 7008-7012 (2011).

107 Chen, R., Ye, Q.-L., He, T. C., Wu, T. & Sun, H. D. Uniaxial tensile strain and exciton–phonon coupling in bent ZnO nanowires. *Applied Physics Letters* **98**, 241916 (2011).

108 Guichuan Xing, N. M., Shuangyong Sun, Swee Sien Lim, Yeng Ming Lam, & Michael Grätzel, S. M., Tze Chien Sum. Long-Range Balanced Electronand and hole-transport lengths in organic-inorganic $CH_3NH_3PbI_3$. *Science* **342**, 344-347 (2013).

109 Samuel D. Stranks, G. E. E., Giulia Grancini, Christopher Menelaou, & Marcelo J. P. Alcocer, T. L., Laura M. Herz, Annamaria Petrozza, Henry J. Snaith. Electron-hole diffusion lengths exceeding 1micrometer in an organometal trihalide perovskite absorber. *Science* **342**, 341-344 (2013).

110 Tian, Y. *et al.* Mechanistic insights into perovskite photoluminescence enhancement: light curing with oxygen can boost yield thousandfold. *Phys*

Chem Chem Phys **17**, 24978-24987 (2015).

111 Hoke, E. T. *et al.* Reversible photo-induced trap formation in mixed-halide hybrid perovskites for photovoltaics. *Chem. Sci.* **6**, 613-617 (2015).

112 Misra, R. K. *et al.* Temperature- and component-dependent degradation of perovskite photovoltaic materials under concentrated sunlight. *J Phys Chem Lett* **6**, 326-330 (2015).

113 Wei Tiwei, C. J., Wang Qian,Hu Yang,Wang Lu,Liu Ziyu,Wu Zijian. Optimization and evaluation of sputtering barrier/seed layer in through silicon via for 3-D integration. *Tsinghua Science and Technology* **19**, 150-160 (2014).

114 Goldstein, J. *et al. Scanning electron microscopy and X-ray microanalysis: a text for biologists, materials scientists, and geologists*. (Springer Science & Business Media, 2012).

115 Schubert, E. F. & Kim, J. K. Solid-state light sources getting smart. *Science* **308**, 1274-1278 (2005).

116 Allen, S. C. & Steckl, A. J. A nearly ideal phosphor-converted white light-emitting diode. *Applied Physics Letters* **92**, 143309 (2008).

117 Hu, Y. *et al.* Piezo-phototronic effect on electroluminescence properties of p-type GaN thin films. *Nano Lett* **12**, 3851-3856 (2012).

118 Yang, Q. *et al.* Largely enhanced efficiency in ZnO nanowire/p-polymer hybridized inorganic/organic ultraviolet light-emitting diode by piezo-phototronic effect. *Nano Lett* **13**, 607-613 (2013).

119 Park, K.-I., Jeong, C. K., Ryu, J., Hwang, G.-T. & Lee, K. J. Flexible and large-area nanocomposite generators based on lead zirconate titanate particles and carbon nanotubes. *Advanced Energy Materials* **3**, 1539-1544 (2013).

120 Lin, L. *et al.* Transparent flexible nanogenerator as self-powered sensor for transportation monitoring. *Nano Energy* **2**, 75-81 (2013).

121 Chen, L., Wong, M.-C., Bai, G., Jie, W. & Hao, J. White and green light emissions of flexible polymer composites under electric field and multiple strains. *Nano Energy* **14**, 372-381, doi:10.1016/j.nanoen.2014.11.039 (2015).

122 Chandra, B. P., Chandra, V. K. & Jha, P. Microscopic theory of elastico-mechanoluminescent smart materials. *Applied Physics Letters* **104**, 031102 (2014).

123 Fan, F.-R., Tian, Z.-Q. & Lin Wang, Z. Flexible triboelectric generator. *Nano Energy* **1**, 328-334 (2012).

124 Bai, G., Zhang, Y. & Hao, J. Tuning of near-infrared luminescence of $SrTiO_3:Ni^{2+}$ thin films grown on piezoelectric PMN-PT via strain engineering. *Sci Rep* **4**, 5724 (2014).

125 Jie, W., Yu Hui, Y., Zhang, Y., Ping Lau, S. & Hao, J. Effects of controllable biaxial strain on the Raman spectra of monolayer graphene prepared by chemical vapor deposition. *Applied Physics Letters* **102**, 223112 (2013).

126 Zheng, R. K. *et al.* Tuning the electrical properties of $La_{0.75}Ca_{0.25}MnO_3$ thin films by ferroelectric polarization, ferroelectric-field effect, and converse piezoelectric effect. *Physical Review B* **74** (2006).

127 Zheng, R. K., Wang, Y., Chan, H. L. W., Choy, C. L. & Luo, H. S. Strain-

mediated electric-field control of resistance in the $La_{0.85}Sr_{0.15}MnO_3$/0.7Pb($Mg_{1/3}Nb_{2/3}$)O_3-0.3$PbTiO_3$ structure. *Applied Physics Letters* **90**, 152904 (2007).

128 Timoshenko, S., Timoshenko, S. & Goodier, J. *Theory of Elasticity, by S. Timoshenko and JN Goodier*. (McGraw-Hill book Company, 1951).

129 Schmidt, O. & Eberl, K. Photoluminescence of tensile strained, exactly strain compensated, and compressively strained $Si_{1-x-y}Ge_xC_y$ layers on Si. *Physical review letters* **80**, 3396 (1998).

130 Hui, Y. Y. *et al.* Exceptional tunability of band energy in a compressively strained trilayer MoS_2 sheet. *Acs Nano* **7**, 7126-7131 (2013).

131 Yang, Q., Wang, W., Xu, S. & Wang, Z. L. Enhancing light emission of ZnO microwire-based diodes by piezo-phototronic effect. *Nano Lett* **11**, 4012-4017 (2011).

132 Fortunato, E., Barquinha, P. & Martins, R. Oxide semiconductor thin-film transistors: a review of recent advances. *Advanced materials* **24**, 2945-2986 (2012).

133 Sahare, S., Dhoble, S., Singh, P. & Ramrakhiani, M. Fabrication of ZnS: Cu/PVA nanocomposite electroluminescence devices for flat panel displays. *Adv. Mater. Lett* **4**, 169-173 (2012).

134 Chandra, B. P. *et al.* Strong mechanoluminescence induced by elastic deformation of rare-earth-doped strontium aluminate phosphors. *Journal of Luminescence* **129**, 760-766 (2009).

135 Hong, Y., Lam, J. W. & Tang, B. Z. Aggregation-induced emission:

phenomenon, mechanism and applications. *Chemical communications*, 4332-4353 (2009).

136 Hu, R., Leung, N. L. & Tang, B. Z. AIE macromolecules: syntheses, structures and functionalities. *Chemical Society Reviews* **43**, 4494-4562 (2014).

137 Wang, J. *et al.* Click synthesis, aggregation-induced emission, E/Z isomerization, self-organization, and multiple chromisms of pure stereoisomers of a tetraphenylethene-cored luminogen. *J Am Chem Soc* **134**, 9956-9966 (2012).

138 Zhang, X. *et al.* Piezofluorochromic properties and mechanism of an aggregation-induced emission enhancement compound containing N-hexyl-phenothiazine and anthracene moieties. *J Phys Chem B* **115**, 7606-7611 (2011).

139 Li, S. *et al.* Understanding the pressure-induced emission enhancement for triple fluorescent compound with excited-state intramolecular proton transfer. *The Journal of Physical Chemistry A* **111**, 11793-11800 (2007).

140 Zhang, R., Jiang, B. & Cao, W. Single-domain properties of $0.67Pb(Mg_{1/3}Nb_{2/3})O_3$-$0.33PbTiO_3$ single crystals under electric field bias. *Applied physics letters* **82**, 787-789 (2003).

141 Jaffe, B., Cook, W. & Jaffe, H. Piezoelectric Ceramics Academic. *New York* (1971).

142 Zheng, R. *et al.* Tuning the electrical properties of $La_{0.75}Ca_{0.25}MnO_3$ thin films by ferroelectric polarization, ferroelectric-field effect, and converse piezoelectric effect. *Physical Review B* **74**, 094427 (2006).

143 Zheng, R. K., Wang, Y., Chan, H. L. W., Choy, C. L. & Luo, H. S. Determination of the strain dependence of resistance in $La_{0.7}Sr_{0.3}MnO_3$/PMN−PT using the converse piezoelectric effect. *Physical Review B* **75** (2007).

144 Sunil K. Singh, K. K., Manish K. Srivastava, Devendra K. Rai, and Shyam B. Rai. Magnetic-field-induced optical bistability in multifunctional Gd_2O_3: Er^{3+}/Yb^{3+} upconversion nanophosphor. *Optics Letters* **35**, 1575-1577 (2010).

145 Akihiro Kojima, K. T., Yasuo Shirai, Tsutomu Miyasaka. Organometal halide perovskites as visible-light sensitizers for photovoltaic. *JACS* (2009).

146 Gottesman, R. *et al.* Photoinduced reversible structural transformations in free-standing $CH_3NH_3PbI_3$ perovskite films. *J Phys Chem Lett* **6**, 2332-2338 (2015).

147 Wang, L., Wang, K. & Zou, B. Pressure-induced structural and optical properties of organometal halide perovskite-based formamidinium lead bromide. *J Phys Chem Lett* **7**, 2556-2562 (2016).

148 Szafranski, M. & Katrusiak, A. Mechanism of pressure-induced phase transitions, amorphization, and absorption-edge shift in photovoltaic methylammonium lead iodide. *J Phys Chem Lett* **7**, 3458-3466 (2016).

149 DeQuilettes, D. W. *et al.* Photo-induced halide redistribution in organic-inorganic perovskite films. *Nat Commun* **7**, 11683 (2016).

150 Shao, Y., Xiao, Z., Bi, C., Yuan, Y. & Huang, J. Origin and elimination of photocurrent hysteresis by fullerene passivation in $CH_3NH_3PbI_3$ planar heterojunction solar cells. *Nat Commun* **5**, 5784 (2014).